

2016

# Cardiorespiratory fitness as a predictor of effective connectivity in the default mode network

---

<https://hdl.handle.net/2144/17015>

*"Downloaded from OpenBU. Boston University's institutional repository."*

BOSTON UNIVERSITY  
SCHOOL OF MEDICINE

Thesis

**CARDIORESPIRATORY FITNESS AS A PREDICTOR OF EFFECTIVE  
CONNECTIVITY IN THE DEFAULT MODE NETWORK**

by

**COREY KRONMAN**

B.S., Boston University, 2013

Submitted in partial fulfillment of the  
requirements for the degree of  
Master of Science

2016

© 2016 by  
COREY KRONMAN  
All rights reserved

Approved by

First Reader

---

Karin Schon, Ph.D.  
Assistant Professor of Anatomy & Neurobiology

Second Reader

---

Ronald Killiany, Ph.D.  
Associate Professor of Anatomy & Neurobiology

## **ACKNOWLEDGMENTS**

I wish to thank Dr. Karin Schon for being an exceptional thesis mentor and first reader, and for her work in the field of aerobic exercise and brain plasticity that made this project possible. I also wish to thank my second thesis reader Dr. Ronald Killiany for his dedication and guidance over the course of this project. Additionally, this project would not have been possible without the technical knowledge and support of Rachel Nauer and Matthew Dunne, who helped to guide me through this project. Further, I would like to recognize all the research staff and students in the Brain Plasticity and Neuroimaging Laboratory of the Department of Anatomy and Neurobiology at Boston University School of Medicine for allowing me to develop and complete this project with their support.

**CARDIORESPIRATORY FITNESS AS A PREDICTOR OF EFFECTIVE  
CONNECTIVITY IN THE DEFAULT MODE NETWORK**

**COREY KRONMAN**

ABSTRACT

Previous work has linked the onset and progression of Alzheimer's Disease (AD) to changes in the Default Mode Network (DMN), including greater atrophy within the hippocampus (HC) as well as diminished functional connectivity and effective connectivity between anatomical DMN structures. Animal models have described the HC as a primary region of interest in studying the effects of exercise on adult neurogenesis and memory performance. Human studies have demonstrated that aerobic exercise leads to greater cardiorespiratory fitness and improved functional connectivity in the DMN for healthy adults. The goal of this study is to go beyond the predictions of human and animal studies to investigate how cardiorespiratory fitness may be used to estimate effective connectivity between the HC and the other DMN structures for young adults using resting state fMRI. Due to the data driven nature of this study, no hypothesis has been formulated. To investigate, data from 25 sedentary young adults was analyzed. Data included a resting state fMRI procedure and a cardiorespiratory fitness test, each taken from part of a larger ongoing clinical trial in the Brain Plasticity and Neuroimaging (BPN) Lab at Boston University (BU). We utilized group independent component analysis (GICA) to identify the regions that define the DMN and Conditional Granger

Causality Analysis (CGCA) to determine effective connectivity between these regions. GICA indicated 9 structural regions in the DMN, consistent with previous work. This resulted in 72 possible instances of effective connectivity. The difference of causal influence between regions was calculated for each pair of DMN regions for CGCA, resulting in 36 possible instances of causal connectivity. Linear regression models were created to analyze the effect of cardiorespiratory fitness on effective connectivity between DMN regions and found 11 linear models which exhibited a significant ( $p > 0.05$ ) relationship. Eight of eleven models involved the left or right hippocampus, showing that greater cardiorespiratory fitness is correlated with changes effective connectivity between the HC and the PCC, MPFC, or LTC. These results provide proof of concept that cardiorespiratory fitness in young adults is associated with changes DMN effective connectivity, particularly involving the hippocampus. This adds to the literature suggesting extended aerobic exercise, which is known to increase cardiorespiratory fitness and has been shown to increase the volume of the HC in older adults, may be neuroprotective of the HC across the lifespan. Further investigation is required to explore how effective connectivity in the DMN changes following an aerobic exercise intervention.

## TABLE OF CONTENTS

TITLE.....	i
COPYRIGHT PAGE.....	ii
READER APPROVAL PAGE.....	iii
ACKNOWLEDGMENTS .....	iv
ABSTRACT.....	v
TABLE OF CONTENTS.....	vii
LIST OF TABLES .....	x
LIST OF FIGURES .....	xi
LIST OF ABBREVIATIONS.....	xii
1. INTRODUCTION .....	1
1.1. Understanding the Resting State.....	4
1.1.1. Discovery .....	4
1.1.2. Resting State Networks.....	6
1.2. The Default Mode Network .....	6
1.2.1. Discovery .....	6
1.2.2. Anatomy.....	7
1.2.3. Functional Theories .....	8
1.3. Neuronal Connectivity Across Distributed Brain Regions.....	10

1.4.	Analyzing Effective Connectivity.....	12
1.5.	Granger Causality Analysis .....	13
1.5.1.	Applications to fMRI Datasets.....	14
1.5.2.	Pairwise Granger Causality Analysis.....	14
1.5.3.	Averaging Techniques and Granger Causality Analysis .....	15
1.5.4.	Conditional Granger Causality Analysis .....	16
1.5.5.	Indirect Measures of Neuronal Activity and Hemodynamic Variability..	16
2.	METHODS .....	18
2.1.	Participants.....	18
2.2.	Cardiorespiratory Fitness Data Acquisition.....	18
2.3.	fMRI Data Acquisition .....	20
2.4.	Data Preprocessing.....	20
2.5.	Group Independent Component Analysis.....	21
2.6.	Default Mode Network Detection and Definition .....	22
2.7.	Default Mode Network Extraction.....	23
2.8.	Conditional Granger Causality Analysis .....	23
2.9.	Statistical Analysis.....	25
3.	RESULTS .....	26
3.1.	VO <sub>2</sub> Max Percentile Represents Cardiorespiratory Fitness .....	26
3.2.	Group Independent Component Analysis Identifies the DMN.....	26
3.3.	Conditional Granger Causality Analysis Defines DMN Causal Influence...	27
3.4.	Cardiorespiratory Fitness Linearly Effects DMN Causal Influence.....	30

4.	DISCUSSION .....	34
4.1.	Default Mode Network Map of Effective Connectivity .....	35
4.2.	Cardiorespiratory Fitness predicts DMN Effective Connectivity.....	35
4.3.	Implications for Preclinical Alzheimer’s Disease.....	37
4.4.	Limitations .....	39
4.5.	Future Directions .....	40
4.6.	Conclusion .....	41
5.	REFERENCES .....	42
6.	CURRICULUM VITAE.....	53

## LIST OF TABLES

Table	Title	Page
1	Study Participant Demographics	19
2	Default Mode Network Regions of Interest	27
3	Average DCI Greater than 50% Relative to the Max	30
4	All Linear Regression Models: Fitness Percentile by Causal Influence Between ROIs	33

## LIST OF FIGURES

Figure	Title	Page
1	Component 19: The Default Mode Network	28
2	Mean Differences of Causal Influence	29
3	Significant Linear Regression Model Plots	32

## LIST OF ABBREVIATIONS

ACSM	American College of Sports Medicine
AD	Alzheimer's Disease
AHN	Adult Hippocampal Neurogenesis
AIC	Akaike Information Criterion
BDNF	Brain Derived Neurotrophic Factor
BIC	Bayesian Information Criterion
BOLD	Blood-Oxygenation Level Dependent
CGCA	Conditional Granger Causality Analysis
CGCM	Conditional Granger Causality Map
DAN	Dorsal Attention Network
DCI	Difference of Causal Influence
DCM	Dynamic Causal Modeling
dMPFC	Dorsal Medial Prefrontal Cortex
DMN	Default Mode Network
fMRI	Functional Magnetic Resonance Imaging
GCA	Granger Causality Analysis
GICA	Group Independent Component Analysis
HRF	Hemodynamic Response Function
IC	Independent Component
ICA	Independent Component Analysis
IHC	Left Hippocampus

IPL	Left Inferior Parietal Lobe
ILTC	Left Lateral Temporal Cortex
MNI	Montreal Neurological Institute
MVAR	Multivariate Vector Autoregressive
MVGC	Multivariate Granger Causality
PC	Principle Component
PCA	Principle Component Analysis
PCC	Posterior Cingulate Cortex
PET	Positron Emission Tomography
PWGCA	Pairwise Granger Causality Analysis
rHC	Right Hippocampus
rIPL	Right Inferior Parietal Lobe
rLTC	Right Lateral Temporal Cortex
ROI	Region of Interest
SIT	Stimulus Independent Thought
VAR	Vector Autoregressive
vMPFC	Ventral Medial Prefrontal Cortex

## 1. INTRODUCTION

According to the 2013-2014 Alzheimer's Disease Progress Report, up to five million adults in the United States are currently living with Alzheimer's Disease (AD) (Aging, 2014). This brings AD to the 6<sup>th</sup> most common cause of death in the United States, costing up to \$215 million dollars each year ("CDC - Healthy Brain Initiative: Alzheimer's Disease - Aging," 2015). By the year 2050, the United States population suffering from AD is expected to grow to 14 million, costing up to \$500 million, making research on AD prevention and therapy more critical than ever (Hebert, Weuve, Scherr, & Evans, 2013).

Numerous studies have linked AD to changes in the Default Mode Network (DMN), the most well defined resting state network (Greicius, Srivastava, Reiss, & Menon, 2004; Hafkemeijer, van der Grond, & Rombouts, 2012; Jones et al., 2011; Koch et al., 2012; Mevel et al., 2011; Rombouts, Barkhof, Goekoop, Stam, & Scheltens, 2005; Sorg et al., 2007; Wang et al., 2013). In particular, the onset and further development of AD is accompanied by diminished glucose metabolism of the, reduced functional connectivity within the DMN, and increased atrophy of the hippocampus (HC) compared to that of a healthy aging population (Greicius et al., 2004; Mevel et al., 2011; Sorg et al., 2007).

Additional studies have shown that long term aerobic exercise may inhibit a number of neurological pathologies related to AD (Burdette, 2010; Li et al., 2014). It has been established in young adult mice that aerobic exercise, such as voluntary treadmill or

wheel running, is associated with a significant increase in adult hippocampal neurogenesis (AHN) (Nokia et al., 2016; H. van Praag, Christie, Sejnowski, & Gage, 1999; H. van Praag, Kempermann, & Gage, 1999). Further studies of aerobic exercise in young adult mouse models have shown that similar improvements in AHN as well as increased vasculature in the HC are correlated with enhancements in cognitive abilities associated with the HC, such as memory and learning (Creer, Romberg, Saksida, Praag, & Bussey, 2010; Marlatt, Potter, Lucassen, & van Praag, 2012; Henriette van Praag, Shubert, Zhao, & Gage, 2005). However, Creer and associates (2010) found that healthy older adult mice performing voluntary wheel running did not experience AHN or hippocampal angiogenesis. Models in which mice did not experience improved AHN did not demonstrate improved learning (Shors et al., 2001) or memory performance (Clelland et al., 2009; Creer et al., 2010).

Human studies in which healthy older adults participated in long term aerobic exercise programs – varying from five weeks to one year – have demonstrated improvements in cerebral blood flow (Burdette, 2010; Maass et al., 2015), increases in white and grey matter brain volumes (Colcombe et al., 2006), increased hippocampal volume (Erickson et al., 2011), and strengthening of functional connectivity in the DMN (Burdette, 2010; Li et al., 2014; Voss et al., 2015) associated with enhancements in cognitive abilities (Voss et al., 2010). Similar studies involving young, initially sedentary adults have demonstrated increased cognitive abilities, such as improved learning and memory task performance, and increased fitness levels as a result of an aerobic exercise program (Griffin et al., 2011; Pereira et al., 2007).

Whiteman and colleagues (2014) examined the relationship between cardiorespiratory fitness in healthy young adults, regardless of their exercise habits, cognitive memory task performance, and a number of growth factors associated with AHN. The Whiteman et al. study demonstrated that recognition memory is positively correlated with the joint interaction between cardiorespiratory fitness of young adults and brain-derived neurotrophic factor (BDNF) (Whiteman et al., 2014), a growth factor responsible for growth, differentiation, and maintenance of neurons (Huang & Reichardt, 2001). Additional studies have demonstrated that cardiorespiratory fitness in healthy young adults is positively correlated with hippocampal memory performance, such as relational memory (Baym et al., 2014), implicit memory, and long term memory (Pontifex et al., 2014). In healthy aging adults, greater cardiorespiratory fitness has been associated with increased HC size, and in turn greater spatial memory task performance (Erickson et al., 2009). Further, cardiorespiratory fitness studies of early clinical AD patients have demonstrated an association between low cardiorespiratory fitness and increased neuronal atrophy in the medial temporal cortex, and parietal cortex (Honea et al., 2009; Vidoni, Honea, Billinger, Swerdlow, & Burns, 2012). This study builds on previous translational research on the interaction of cardiorespiratory fitness and exercise with neurological pathologies of AD by exploring the use of cardiorespiratory fitness in young adults to predict effective connectivity between regions of the DMN.

## **1.1. Understanding the Resting State**

It is well known that the brain experiences metabolic and neurological activity at all times (Rosazza & Minati, 2011). This begs the question, what is happening when the brain goes unstimulated by the outside world? The brain is in the resting state. The resting state defines the activity that is not directed by the outside world. In other words, when the brain is in the resting state, it does not receive input from the external environment, nor does it supply output to the environment. Instead, the resting state brain is guided by spontaneous intrinsic activations (Raichle, 2015; Rosazza & Minati, 2011). This commonly occurs when the brain is in a wakeful state and experiencing a task-negative environment (Rosazza & Minati, 2011). Interestingly, investigators have identified resting state networks, particularly the Default Mode Network, in individuals across a wide spectrum of consciousness including healthy control states, minimally conscious states, comatose states, vegetative states, and during locked-in syndrome (Vanhaudenhuyse et al., 2010). However, the resting state is not exhibited in brain dead patients (Mantini & Vanduffel, 2013; Rosazza & Minati, 2011; Vanhaudenhuyse et al., 2010). This evidence suggests that resting state activity may maintain the conscious experience.

### ***1.1.1. Discovery***

The increase in regional activity while in an introspective state was first recognized by David Ingvar (1979; Ingvar & Franzén, 1974). He noticed greater blood flow in frontal brain regions during what he called "spontaneous conscious mentation."

Later, Shulman et al. (1997) formally identified a distinct set of brain regions with diminished activity during active tasks in comparison to during resting state conditions. The data came from a set of nine Positron Emission Tomography (PET) studies. The investigators who designed these studies asked participants to complete tasks requiring focused attention on an external environment. The control task placed participants in resting state conditions either with their eyes closed, or fixated on a static visual stimulus. The brain regions that display diminished activity during active tasks define what Shulman et al., and many other investigators have termed resting state network (Raichle, 2015). The results of these studies have been reproduced using both functional Magnetic Resonance Imaging (fMRI) and PET methods, displaying consistent activations throughout the resting state network (R. L. Buckner, Andrews-Hanna, & Schacter, 2008; Raichle, 2015).

Today, fMRI is the most prominent technique used to acquire resting state data (Biswal et al., 2010; Mevel et al., 2011; Rosazza & Minati, 2011). fMRI takes advantage of the magnetic moments of Hydrogen atoms in deoxygenated Hemoglobin (Faro & Mohamed, 2010; Gore, 2003). By applying gradient echo techniques in a strong, static magnetic field sensitive to deoxyhemoglobin, an fMRI machine can measure the Blood-Oxygenation-Level Dependent (BOLD) contrast in the brain, which reflects local field potentials, a measure of coherent neuronal population activity (Logothetis, 2003). Therefore, BOLD provides a method to view neuronal activity. To stimulate resting state activity in an fMRI machine, study participants are directed to lay still and either close

their eyes or stare at a crosshair on a screen, stay awake, and let their mind wander while the machine collects data (Cole, 2010; Rosazza & Minati, 2011).

### ***1.1.2. Resting State Networks***

With varying methods used to identify resting state networks, researchers have now defined distinct sets of brain regions that are activated in concert during the resting state (Beckmann, DeLuca, Devlin, & Smith, 2005; Cole, 2010; Damoiseaux et al., 2006; De Luca, Beckmann, De Stefano, Matthews, & Smith, 2006; Liao et al., 2009; Raichle, 2015; Rosazza & Minati, 2011). A list of common networks identified includes the central executive network, the self referential network, the dorsal attention network (DAN), the auditory network, the sensorimotor network, the visual processing network, the core network, and the default mode network (DMN) (Liao et al., 2009). Of these resting state networks, the DMN was the first to be discovered; therefore, it has received the most attention from investigators. (R. L. Buckner et al., 2008).

## **1.2. The Default Mode Network**

### ***1.2.1. Discovery***

The DMN was an inadvertent discovery. Investigators regularly collected resting state data as a control to contrast the data collected during active task performance. The increasing use of PET in the 1990s revealed brain regions exhibiting greater blood flow during the passive resting state control tasks than during the active tasks, eventually

intriguing investigators to study these regions in greater depth (R. L. Buckner et al., 2008).

Such studies describe DMN activity as low or suppressed during active tasks with external inputs, such as attention demanding cognitive tasks, and high during passive resting conditions (i.e. “fixation” condition or “null” events). In other words, the DMN peaks in activity when an individual's attention is focused internally. With this in mind, we turn to discuss the anatomy of the DMN before continuing to describe the DMN function.

### ***1.2.2. Anatomy***

The DMN is a neuronal network system. Like other networks, such as the sensory system and the motor system, the DMN can be described by anatomical and functional models. As such, it is comprised of a series of hubs and nodes, which exchange information between each other and with external networks (R. L. Buckner et al., 2008). Understanding the anatomy of the DMN can assist in our understanding of its function.

The DMN anatomy has been determined by previous studies using a variety of techniques, producing consistently similar results (R. L. Buckner et al., 2008; Raichle, 2015). For example, Shulman et al. (1997) used PET to determine blocked task induced deactivations, Shannon (R. L. Buckner et al., 2008) used fMRI to determine event related task induced deactivations in the DMN, and Greicius et al. (2004) used fMRI to analyze low frequency, spontaneous correlations for functional connectivity that are characteristic of the DMN. The results of these studies exhibit a consistent anatomical structure in the

DMN. According to meta analyses of DMN anatomy, including those stated above, the medial prefrontal cortex (MPFC), posterior cingulate cortex (PCC), and the inferior parietal lobule (IPL) are major hubs in the DMN (Andrews-Hanna, 2012; R. L. Buckner et al., 2008; Mantini & Vanduffel, 2013; Raichle, 2015). Further, the HC, a brain area critical in episodic learning and memory (Eichenbaum, 2000), appears as a component of the DMN in many studies (R. L. Buckner et al., 2008). Although the HC is not consistently defined as a DMN component, the argument for its involvement in the DMN is strengthened by the functional role of both the HC and the DMN in memory retrieval (R. L. Buckner et al., 2008; Eichenbaum, 2000). Finally, each of the above studies revealed the lateral temporal cortex (LTC) to be involved in the DMN (Andrews-Hanna, 2012; R. L. Buckner et al., 2008).

### ***1.2.3. Functional Theories***

Current research provides two theories defining the function of the DMN: the sentinel hypothesis and the internal mentation hypothesis (R. L. Buckner et al., 2008; Gilbert, Dumontheil, Simons, Frith, & Burgess, 2007; Mantini & Vanduffel, 2013; Mevel et al., 2011). It is likely that the DMN functions as a mixture of these two ideas.

The sentinel hypothesis suggests that the role of the DMN is to survey the external environment, scanning for uncommon, or unusual information (R. L. Buckner et al., 2008; Hahn, Ross, & Stein, 2007; Mantini & Vanduffel, 2013). According to this theory, during resting state conditions an individual experiences a low level of focused attention while passively exploring the external environment in a state of “watchfulness”

(Gilbert et al., 2007). The sentinel hypothesis is supported by a variety of brain imaging and patient studies. For example, Hahn et al. (2007) showed greater DMN activation during sensory processing task when individuals were asked to focus broadly compared to when they were asked to focus on a distinct location.

However, the sentinel hypothesis does not take into account the DMN regions involved in the memory system, specifically, the HC. Recall that the HC is inconsistently defined as a DMN brain region. The cause may be that the HC is not consistently recruited with the rest of the DMN brain regions. According to one study, the PCC, left IPL, and left anterior MPFC play an important role in the retrieval of familiar memories and words (Kim, 2016). Note that these are all DMN brain regions. The same study also noted that the HC exhibited activity during familiar memory retrieval, but not during familiar word retrieval. Another study noted that the hippocampus behaves as a DMN brain region during memory retrieval, an internally stimulated process, but not during memory encoding, an externally stimulated process (Huijbers, Pennartz, Cabeza, & Daselaar, 2011; Kim, 2015).

According to the internal mentation hypothesis, we experience spontaneous cognition via the DMN during the resting state (R. L. Buckner et al., 2008; Mantini & Vanduffel, 2013). Spontaneous cognition involves processes such as daydreaming, mind wandering, fantasy, introspection, and thought when an individual is not engaged in a task that requires active, intentional thought (R. L. Buckner et al., 2008). Many of these processes involve memory retrieval, accounting for the HC as a DMN brain region.

Spontaneous cognition consists of "stimulus independent thoughts" (SITs), meaning thoughts are not determined by an external stimulus. SITs are often reported to be thoughts about the past and future or self-referential thoughts (R. L. Buckner et al., 2008; Mantini & Vanduffel, 2013; Raichle, 2015). Supporting the internal mentation hypothesis, Binder et al. (1999) demonstrated that the frequency of SITs, as well as DMN activity are both greater during the resting state than during externally motivated activity. Further, Mason et al. (2007) showed that an increase in the number of SITs is correlated with an increase in MPFC and PCC activity. It is important to note that SITs occur during active task activities as well as resting state activities (R. L. Buckner et al., 2008). Investigators have demonstrated two notable changes when SITs occur during active task activities (Weissman, Roberts, Visscher, & Woldorff, 2006). One, SITs may be predicted by a decrease in DAN activity, suggesting greater DMN activity when attention to the external world falls. Two, SITs are accompanied by increased activity in the PCC, a hub of the DMN.

### **1.3. Neuronal Connectivity Across Distributed Brain Regions**

Traditionally, fMRI studies attempt to identify brain regions associated with specific functions (Deshpande & Hu, 2012). However, many high level functions cannot be explained by such studies. One theory suggests that higher level functions are controlled by interactions between a variety of brain regions (Deshpande & Hu, 2012). These interactions are the basis for various brain connectivity theories. We must be able to differentiate between the theories of anatomic, functional, and effective connectivity

(Horwitz, 2003). To add to the complexity, many investigators differ in their interpretations of each form of connectivity. Therefore, each form of connectivity will be described in this section for reference to this paper.

Anatomical connectivity refers to the physical structure of neuronal connections at the microscopic level (Horwitz, 2003). It involves pre-synaptic neurons, synapses, and receptors, and post-synaptic neurons (Sporns, 2007). Although fMRI does not measure anatomical connectivity, knowledge of anatomical connectivity, such as that derived from tracer studies in monkeys, can inform functional and effective connectivity models.

Functional, or instantaneous, connectivity is measured by comparing a set of neuronal time course data. If the neuronal activity is statistically correlated across time, the set neurons or regions are functionally correlated (Deshpande & Hu, 2012; Friston, 2011; Horwitz, 2003; Liao et al., 2009). Functional connectivity can occur via an external input to the system that activates multiple brain regions, or it may be from a synaptic pathway within other neuronal regions of the system that continues to multiple output regions (Friston, 2011). The two most common methods to examine functional connectivity are seed-based methods and independent component analysis (ICA). Seed-based analysis is a hypothesis driven method. When an investigator hypothesizes that functional connectivity may change if a specific brain region is manipulated, this brain region serves as the seed. Seed-based functional connectivity analysis then examines the correlation of other brain regions with the seed to determine the functional connectivity for a neuronal network. For this reason, seed-based analysis cannot be used as an exploratory technique to define brain regions within a network (Joel, Caffo, van Zijl, &

Pekar, 2011). In contrast, ICA does not involve a hypothesis; it is a data-driven method of functional connectivity analysis. Instead of using a seed voxel for comparison, ICA makes use of correlation coefficients across all voxels (Deshpande & Hu, 2012; Friston, 2011). In this way, ICA compares connectivity between voxels as well as between patterns of voxels to classify brain networks by region (Joel et al., 2011).

Effective, or causal, connectivity between brain regions implies a causal relationship between activity of the regions involved (Deshpande & Hu, 2012; Friston, 2011; Friston & others, 1994). This model of connectivity relies on neural interactions in the form of correlations between neuronal activity across time (Friston, 2011). Effective connectivity has been analyzed using statistical methods such as Structural Equation Modeling (SEM), Dynamic Causal Modeling (DCM), and Granger Causality Analysis (GCA) (Deshpande & Hu, 2012; Roebroeck, Formisano, & Goebel, 2011). These methods make use of complex statistical analysis to allow investigators to examine the neuronal activity hidden behind functional connectivity. Such analysis alludes to the directionality of the flow of neuronal information in the brain as it interacts with itself (Friston, 2011).

#### **1.4. Analyzing Effective Connectivity**

Currently, fMRI is the gold standard of use for neuronal connectivity measurements (Horwitz, 2003; Roebroeck, Formisano, & Goebel, 2005; Roebroeck et al., 2011). The most effective techniques applicable to examining effective connectivity with fMRI data are Dynamic Causal Modeling (DCM) and Granger Causality Analysis

(GCA). DCM and GCA both analyze temporal causality, but they have major methodological differences (Roebroek et al., 2011). DCM uses confirmatory methods. It applies a deterministic mathematical model to confirm or deny the validity of a specific model of connectivity; therefore, it is hypothesis driven. In contrast, GCA takes advantage of an exploratory approach. GCA analyzes data using a linear autoregressive model to examine each possible model of connectivity for statistical significance. GCA also includes a stochastic factor, permitting variation in the results that may not be explained by the original input (Roebroek et al., 2011). Therefore, GCA does not require prior knowledge on the physical representation of our model of connectivity as an input.

### **1.5. Granger Causality Analysis**

In 1969, Clive Granger suggested a statistical method using a vector-autoregressive (VAR) model to calculate causality between two time-series (Granger, 1969). Since then, researchers have modified Granger's methods to analyze a variety of complex causal relationships (Deshpande, Santhanam, & Hu, 2011; Eye, Wiedermann, & Mun, 2013; Geweke, 1984; Liao et al., 2009; Tang, Bressler, Sylvester, Shulman, & Corbetta, 2012). In this section we will look at Granger Causality Analysis and a subset of modifications that will be useful in our analysis.

Using the original method defined by Granger (1969), causality between two time-series is determined by a comparison of two models: the constrained model and the unconstrained model. Consider two time-series, A and B. The constrained model attempts to predict the future value of B using past values of B. The unconstrained model attempts

to predict the future value of B using past values of both A and B. The two models are then compared. (Bressler & Seth, 2011; Deshpande & Hu, 2012; Deshpande, LaConte, James, Peltier, & Hu, 2009; Deshpande et al., 2011; Eye et al., 2013; Granger, 1969; Roebroek et al., 2005). A Granger-causes B if the unconstrained model is significantly more accurate in predicting future values of B than the constrained model.

### ***1.5.1. Applications to fMRI Datasets***

When an fMRI dataset is collected each volumetric pixel, or voxel, represents one time-series vector. Each vector is concatenated to form a matrix, which represents the scanned brain region over the duration of data collection. GCA, as defined by Granger (1969), is limited to analyzing a bivariate time series relationship. When more than two time-series exist in a multivariate system, a relationship between two variables may be determined by third variable or a set of variables. This renders traditional GCA ineffective in determining direct temporal causality (Bressler & Seth, 2011; Granger, 1969; Liao et al., 2009; Tang et al., 2012). Multivariate analyses are required to analyze effective connectivity among three or more voxels of a fMRI dataset.

### ***1.5.2. Pairwise Granger Causality Analysis***

One way to analyze multivariate fMRI datasets using GCA is pairwise granger causality analysis (PWGCA). This method analyzes each potential causal relationship voxel by voxel (Tang et al., 2012; Zhou et al., 2009). However, PWGCA has been

criticized as ineffective in analyzing multivariate systems. To start, analyzing a multivariate system voxel-by-voxel requires an abundant amount of time and computing power given that an fMRI series can contain over 100,000 voxels per image acquisition (Tang et al., 2012; Zhou et al., 2009). Moreover, when used with multivariate systems, PWGCA may lead to patterns of false significance between time-series that do not share a causal relationship (Barnett & Seth, 2014; Zhou et al., 2009). Consider a three time series: A, B, and C. By pairwise calculation, if A causally influences B, and B causally influences C, PWGCA is likely to find a causal influence from A to C even it does not directly exist. This relationship between A and C is termed a “lagged dependency,” and may grow more complicated as the number of variables grows. (Barnett & Seth, 2014).

### ***1.5.3. Averaging Techniques and Granger Causality Analysis***

Another way to use GCA to analyze multivariate fMRI datasets takes advantage of averaging techniques (Zhou et al., 2009). This works by creating an average time-series vector from a set of voxels within a region of interest (Goebel, Roebroeck, Kim, & Formisano, 2003; Roebroeck et al., 2005; Zhou et al., 2009). This leaves each region of interest represented by one time-series vector, reducing the dimensionality of the matrix representing the fMRI dataset. With a reduced matrix, PWGCA or Conditional Granger Causality Analysis (CGCA; see below) can be applied more easily. However, averaging results in a major loss of information, modifying the outcome of PWGCA (Zhou et al., 2009).

#### ***1.5.4. Conditional Granger Causality Analysis***

To analyze multivariate systems more effectively, Geweke (1984) modified GCA to account for tertiary variables that may moderate the relationship between the two variables in question. This computation is termed conditional Granger causality analysis (CGCA) (Bressler & Seth, 2011; Geweke, 1984; Liao et al., 2009; Tang et al., 2012; Wei et al., 2015). CGCA calculates significant causal relationships between two time series in a multivariate system by conditionally accounting for the effects of all potential tertiary time series. In this way, defining significance in the causal relationship between two time courses is conditional on all other time courses in the system. CGCA takes advantage of multivariate autoregressive (MVAR) modeling as detailed in the original paper by Geweke (1984). To summarize the idea, imagine two time courses X and Y, and a set of all other time courses in the system represented by Z. If the past of X, Y, and Z, together, can predict the future of Y better than the past of Y and Z, then X conditionally Granger-causes Y.

#### ***1.5.5. Indirect Measures of Neuronal Activity and Hemodynamic Variability***

Recall that the fMRI provides the hemodynamic response (HDR), which is a measure of the BOLD response. The causality we wish to analyze is that of the neuronal activity (Deshpande & Hu, 2012; Deshpande et al., 2011; Liao et al., 2009). The neuronal activity can be uncovered by deconvolving the BOLD response with a hemodynamic response function (HRF), which is a model of the HDR (Deshpande & Hu, 2012; Liao et al., 2009). To estimate the neuronal activity, investigators approximate the HRF using predetermined biological data and probabilistic filtering (Deshpande & Hu, 2012). Once

HDR is deconvolved with the HDF, the estimated neuronal activity data remains. The HRF presents additional challenges as it varies by region across the brain, making it difficult to predict. (Deshpande & Hu, 2012; Roebroek et al., 2011). The HRF spatial variability is likely to have a negative impact on the GCA of the fMRI data as it manifests itself as differences in time to peak, and peak width between regions.

However, simultaneous EEG-fMRI experiments on monkeys demonstrate the resting state changes in the BOLD response are caused by changes in resting state neuronal activity (Deshpande et al., 2011; Leopold, Murayama, & Logothetis, 2003; Shmuel & Leopold, 2008). Further, Deshpande and Hu (2012) argue that because the spatial variability is caused by structural differences from varying vasculature in the brain, the spatial variability should not change across time at each particular brain region. Therefore, any observed temporal variation must come from a change in neuronal activity, not from spatial hemodynamic variability. These findings suggest performing GCA on BOLD data may be a close enough estimate to determine causality in fMRI data (Deshpande & Hu, 2012). Further investigation is needed in to confirm this idea.

## **2. METHODS**

### **2.1. Participants**

Participant data for this study was retrieved from the Brain Plasticity and Neuroimaging Laboratory at the Boston University School of Medicine as a part of a larger study on effects of cardiovascular exercise on human memory and hippocampal memory function. Participants in the larger study were English language speakers between the ages of 18 and 35 or 55 and 85 years. In addition, participants self-reported no neurological or psychiatric conditions at the time of the study, and have been living sedentary lifestyles (as defined by less than 30 minutes of moderate intensity physical activity 3 days per week) for at least 3 months. All participants provided signed, informed consent prior to participation in the study; and all study procedures followed the guidelines set by the Code of Ethics of the World Medical Association and were approved by the Boston University Medical Campus Institutional Review Board.

Twenty-six study participants were pulled from the database who completed both a baseline resting state fMRI procedure and a cardiorespiratory fitness test. One participant was excluded from analysis due to excessive head motion during the fMRI scanning process. This resulted in a total of 25 participants included in data analysis. See Table 1 for relevant participant demographics.

### **2.2. Cardiorespiratory Fitness Data Acquisition**

Cardiorespiratory fitness was determined by estimating  $VO_2$  max using a modified Balke protocol on a treadmill where walking speed was fixed while grade was

increased incrementally (American College of Sports Medicine, Thompson, Gordon, & Pescatello, 2010; Cooper & Storer, 2001). Using data collected during the modified Balke treadmill test,  $VO_2$  max for each participant was approximated by extrapolating to the age and sex predicted maximum heart rate from a plot of heart rate vs.  $VO_2$ , where  $VO_2$  was calculated using the American College of Sports Medicine (ACSM) metabolic equation for Gross  $VO_2$  for walking:

$$VO_2 = 0.1 \text{ ml}/\text{kg} \cdot \text{min} \times S + 1.8 \text{ ml}/\text{kg} \cdot \text{min} SG + 3.5 \text{ ml}/\text{kg} \cdot \text{min}$$

in which  $VO_2$ ,  $S$ , and  $G$  represent gross oxygen consumption ( $\text{ml} / (\text{kg} \cdot \text{min})$ ), speed ( $\text{m}/\text{min}$ ), and the percent of the treadmill grade as a fraction, respectively (American College of Sports Medicine et al., 2010).  $VO_2$  max percentile was determined for each participant based on  $VO_2$  max norms by age and sex.

**Table 1. Study Participant Demographics**

This table represents the participant demographics relevant to this study

<b>N</b>	<b>25</b>
$N_{\text{Female}}$	16
$N_{\text{Right Handed}}$	21
<b>Age Range</b>	20 – 33 years
Mean $\pm$ SD	26 $\pm$ 3.8 years
<b><math>VO_2</math> Max Percentile Range</b>	2% – 96%
Mean $\pm$ SD	52% $\pm$ 28%

### **2.3. fMRI Data Acquisition**

A 3-Tesla Philips Achieva scanner, paired with an 8-channel SENSE head coil, was used to collect structural and functional imaging data at the Boston University Center for Biomedical Imaging in Boston, MA, USA. For each participant, a structural T<sub>1</sub>-weighted magnetization prepared rapid acquisition gradient echo (MP-RAGE) structural image was obtained (SENSitivity Encoding P reduction: 1.5, S reduction: 2; TR = 6.8 ms, TE = 3.1 ms, flip angle = 9 °, Field of View = 25 cm, Matrix Size = 256 × 254; 150 slices, resolution = 0.98 mm × 0.98 mm × 1.22 mm).

Additionally, 200 functional BOLD volumes were obtained during the 10-minute resting state fMRI scan for each participant. The BOLD images were obtained with a T<sub>2</sub>\*-weighted echo-planar imaging sequence using an in plane acquisition resolution of 3.3125 mm<sup>2</sup> and slice thickness of 3.3125 mm (TR = 3000 ms; TE = 30 ms; flip angle = 80°; Field of View = 212 mm × 199 mm; matrix size = 64 × 59; 48 slices per volume).

### **2.4. Data Preprocessing**

The fMRI data was preprocessed with the SPM8 software package (Statistical Parametric Mapping, Wellcome Department of Cognitive Neurology, London, UK) an extension of MATLAB 8.1 (R2013a; The MathWorks Inc., Natick, MA, USA). First, the T<sub>1</sub> anatomical and BOLD functional images were reoriented to define the anterior commissure as the point of origin. The individual functional images were then realigned using a 6-parameter rigid-body alignment procedure to correct for translational and rotational head motion. All functional images were warped by less than ±2 mm and/or

$\pm 2^\circ$ . Following realignment individual anatomical images were co-registered to the mean functional image. The co-registered anatomical image was re-sliced to a  $2 \text{ mm} \times 2 \text{ mm} \times 2 \text{ mm}$  voxel resolution and spatially normalized to the Montreal Neurological Institute (MNI) space. In doing so, the define transformation parameters were defined to normalize the individual functional images to the MNI space after. Prior to normalization, the functional images were also re-sliced to a voxel resolution of  $2 \text{ mm} \times 2 \text{ mm} \times 2 \text{ mm}$ . Finally, all images were smoothed with a full-width at half-maximum of 8mm by a three dimensional Gaussian kernel.

## **2.5. Group Independent Component Analysis**

The Group ICA/IVA of fMRI Toolbox v3.0a (GIFT) (Rachakonda, Egolf, Correa, & Calhoun, 2007) was used to spatially decompose the preprocessed images into independent components (ICs). The algorithm first implemented data reduction using a two-step principle component analysis (PCA) to reduce the data dimensions. The first step temporally reduced data from 200 principle components (PCs) for each participant to 38 concatenated PCs. The second step temporally reduced the 38 concatenated PCs of each individual to 25 PCs representing all participants. Next, Group Independent Component Analysis (GICA) was performed using the Extended Infomax Algorithm as performed in previous studies (Miao, Wu, Li, Chen, & Yao, 2011). The ICASSO software included in GIFT was used to confirm statistical stability by running GICA analysis 20 times (Himberg & Hyvärinen, 2003). GICA produced the mean (ICs) aggregated for all participants as well as their corresponding aggregate time courses

(Rachakonda et al., 2007). The time courses and ICs from GICA were used to back reconstruct the time courses and ICs of each individual participant. The back reconstructed ICs and time courses, represented in arbitrary units, were then calibrated by implementing z-scores. Finally, group statistics were performed over all participants, providing mean, standard deviation, and t-statistic maps for each IC.

## **2.6. Default Mode Network Detection and Definition**

The DMN was identified from the 25 ICs using a combination of frequency analysis, visual inspection, and correlation with a DMN template (*'ref\_default\_mode.nii'*) provided by GIFT (Kelly et al., 2010; Miao et al., 2011; Rachakonda et al., 2007). Eliminated ICs displayed at least one of the following: a ring-like pattern near the cerebrospinal fluid, large bilateral clusters in the frontal polar regions, “speckled” patterns, large groups of significant voxels in the superior sagittal sinus, large clusters in white matter, frequencies outside the range of 0.01 Hz to 0.1 Hz, saw tooth time course patterns, abrupt spikes in the time course pattern, or less than a 25% correlation with the DMN template provided by GIFT (Kelly et al., 2010). In addition, to be defined as the DMN component, the IC had to overlap with the PCC, the IPLs and the MPFC (R. L. Buckner et al., 2008; Franco, Pritchard, Calhoun, & Mayer, 2009; Raichle, 2015; Shulman et al., 1997).

Using the selected DMN component, nine DMN regions of interest (ROIs) were identified: the ventral medial prefrontal cortex (vMPFC), dorsal medial prefrontal cortex (dMPFC), PCC, left inferior parietal lobule (lIPL), right inferior parietal lobule (rIPL), left

lateral temporal cortex (lLTC), right lateral temporal cortex (rLTC) , left hippocampus (lHC), and right hippocampus (rHC) (R. L. Buckner et al., 2008; Damoiseaux et al., 2006; Fox et al., 2005; Franco et al., 2009; Mazoyer et al., 2001; Raichle, 2015; Shulman et al., 1997). Each ROI was identified using the xjView toolbox (<http://www.alivelearn.net/xjview>) for SPM8 (Miao et al., 2011). The one-sample t-test map ( $p = 0.05$ , FDR) of the DMN component created in GIFT was imported and overlaid on an anatomically labeled map of the DMN. The coordinates of the local maximum within each of the nine ROIs were identified and recorded as the center for each ROI.

## **2.7. Default Mode Network Extraction**

Coordinates of the identified ROI centers were imported to the MarsBaR ROI toolbox for SPM (Brett, Anton, Valabregue, & Poline, 2002). A group-specific DMN template was built by creating a sphere of radius 10 mm to represent each ROI. The template was laid over the preprocessed functional images of each participant to identify voxels for time course extraction. Following voxel-by-voxel extraction, each ROI was subjected to PCA (using the *pca* function of MATLAB 8.1 (R2013b)) to reduce the dataset to a single time course.

## **2.8. Conditional Granger Causality Analysis**

To examine the effects of cardiorespiratory fitness on causal influence within the DMN, a mathematical model that would account for noise in the neuronal time series was

required. The mathematical model must have also been data driven, as the analysis lacked a physical model-based hypothesis. Rather, it was based on the correlation of time courses. For these reasons, use of the stochastic factor and an exploratory approach made CGCA the best technique to examine the effects of cardiorespiratory fitness on causal influence in the DMN.

Conditional Granger Causality Analysis (CGCA) was performed using the Multivariate Granger Causality (MVGC) toolbox (Barnett & Seth, 2014). The model order was determined using both Bayesian Information Criterion (BIC) and Akaike Information Criteria (AIC). After model order estimation, Vector Autoregressive (VAR) Model Estimation was performed to identify the VAR coefficient matrix ( $A_k$ ), and the residuals covariance matrix ( $\Sigma$ ) from the ROI time course data. The VAR coefficients matrix ( $A_k$ ) and the residuals covariance matrix ( $\Sigma$ ) were used to find the autocovariance sequence ( $\Gamma_k$ ) by reverse solving the Yule-Walker Equation (Barnett & Seth, 2014). Conditional granger causality was first calculated in the frequency domain from the autocovariance sequence. A band pass filter (0.01 Hz – 0.10 Hz) was applied to the spectral granger causality matrix ( $f(\lambda)$ ) prior to fourier transformation, creating the time domain conditional granger causality matrix ( $F$ ). P-values for each granger causality term were calculated to determine significance ( $p < 0.05$ ). Causal influence between two ROIs was determined by subtracting the conditional granger causality term between the two ROIs in one direction from the conditional granger causality term between the two ROIs in the opposite direction. This term was defined as the difference of causal influence (DCI). A DMN map was created to represent the mean DCI across all

participants using the NodeXL software package for Microsoft Excel (<http://nodexl.codeplex.com/>).

## **2.9. Statistical Analysis**

VO<sub>2</sub> max percentile was analyzed as a predictor of the DCI between each pair of DMN ROIs while controlling for physiological sex and handedness on a group level. The *LinearModel.fit* function in MATLAB 8.1 (R2013b) was used to create a linear regression model for each pair of ROIs accounting for each of the above named covariates as well as their two-way interactions. VO<sub>2</sub> max percentile was represented as a continuous range from 0 to 100%, physiological sex was interpreted as a binary input (male or female), and handedness was given as a binary input (left handed or right handed). Handedness and physiological sex were maintained as a controlled constant while analyzing the relationship between VO<sub>2</sub> max percentile and estimated DCI using ordinary least squares regression.

After determining the linear regression model for each ROI pair, the standard error, t-statistic, r-squared value, and p-value were calculated across all participants. A linear regression model was determined to be statistically significant if  $p > 0.05$ . Significant linear regression models were plotted (See Figure 3).

### 3. RESULTS

#### 3.1. VO<sub>2</sub> Max Percentile Represents Cardiorespiratory Fitness

Cardiorespiratory fitness testing was successfully carried out with 25 young, healthy participants. Participant VO<sub>2</sub> max percentile ranged from the 2<sup>nd</sup> percentile to the 96<sup>th</sup> percentile for age and gender predicted VO<sub>2</sub> max as calculated using data collected with the modified Balke protocol in conjunction with the ACSM metabolic equation for gross VO<sub>2</sub> for walking. The mean VO<sub>2</sub> max percentile over all participants is  $51.9 \pm 28.6\%$  (Mean  $\pm$  Standard Deviation). The median VO<sub>2</sub> max percentile is 53%. VO<sub>2</sub> max percentile did not differ significantly by physiological sex ( $p = 0.31$ ) or by handedness ( $p = 0.42$ )

#### 3.2. Group Independent Component Analysis Identifies the DMN

GICA, as performed by GIFT, decomposed the resting state fMRI functional images into 25 spatially mapped ICs. Component 19, displayed in Figure 1, was defined as the DMN after a visual review of all 25 spatial IC maps. This IC displayed a greater correlation, 0.56, with the DMN template provided by GIFT (*ref\_default\_mode.nii*) than any other IC. The DMN power spectrum was between 0.1 Hz and 0.01 Hz, with a strong peak at 0.02 Hz. Using the aal atlas component of xjView for SPM, nine ROIs were identified in the DMN including the PCC, rIPL, lIPL, rLTC, lLTC, rHC, lHC, vMPFC, and dMPFC. The peak t-statistic within each cluster was identified and defined as the center for each ROI. With an assumed false discovery rate (FDR) of 0.05 (providing a

minimum t-statistic threshold of 2.58), the peak t-statistic ranged from 4.24 to 29.74, and ROI cluster sizes varied from 28 voxels to 1438 voxels. See Table 2 for peak coordinates, t-statistics, and cluster size of the DMN ROIs identified.

The peak t-statistic coordinates for each ROI were used to create spheres (radius = 10 mm) defining the individual ROI voxels for time course extraction of each participant's functional BOLD data. PCA defined a single activation time course for each of the nine ROIs extracted from each participant, resulting in nine PCs for each of the 25 participants.

**Table 2. Default Mode Network Regions of Interest**

This table lists the anatomical structures defined by ROI analysis of the DMN. The threshold t statistic was defined as 2.58, where the false discovery rate  $p = 0.05$ .

ROI	Peak Coordinates (x, y, z)	Peak t Statistic	Cluster size (number of voxels)
PCC	(6, -54, 20)	29.74	1438
lIPL	(-50, -66, 26)	15.89	259
rIPL	(44, -70, 36)	16.33	122
lLTC	(-44, 14, -28)	5.23	67
rLTC	(44, 12, -28)	4.24	28
lHC	(-22, -12, -16)	6.08	153
rHC	(24, -8, -14)	5.16	43
vMPFC	(0, 64, -4)	5.91	253
dMPFC	(2, 56, 28)	4.70	690

### 3.3. Conditional Granger Causality Analysis Defines DMN Causal Influence

CGCA was performed across all PCs for each participant using a model order of one, as estimated using both AIC and BIC. Conditional Granger Causality Maps

(CGCMs) were created to analyze conditional granger causality between each set of distinct ROIs. Figure 3 shows the network map created from averaging the CGCMs of all 25 participants. The arrow direction indicates the difference of causal influence from one

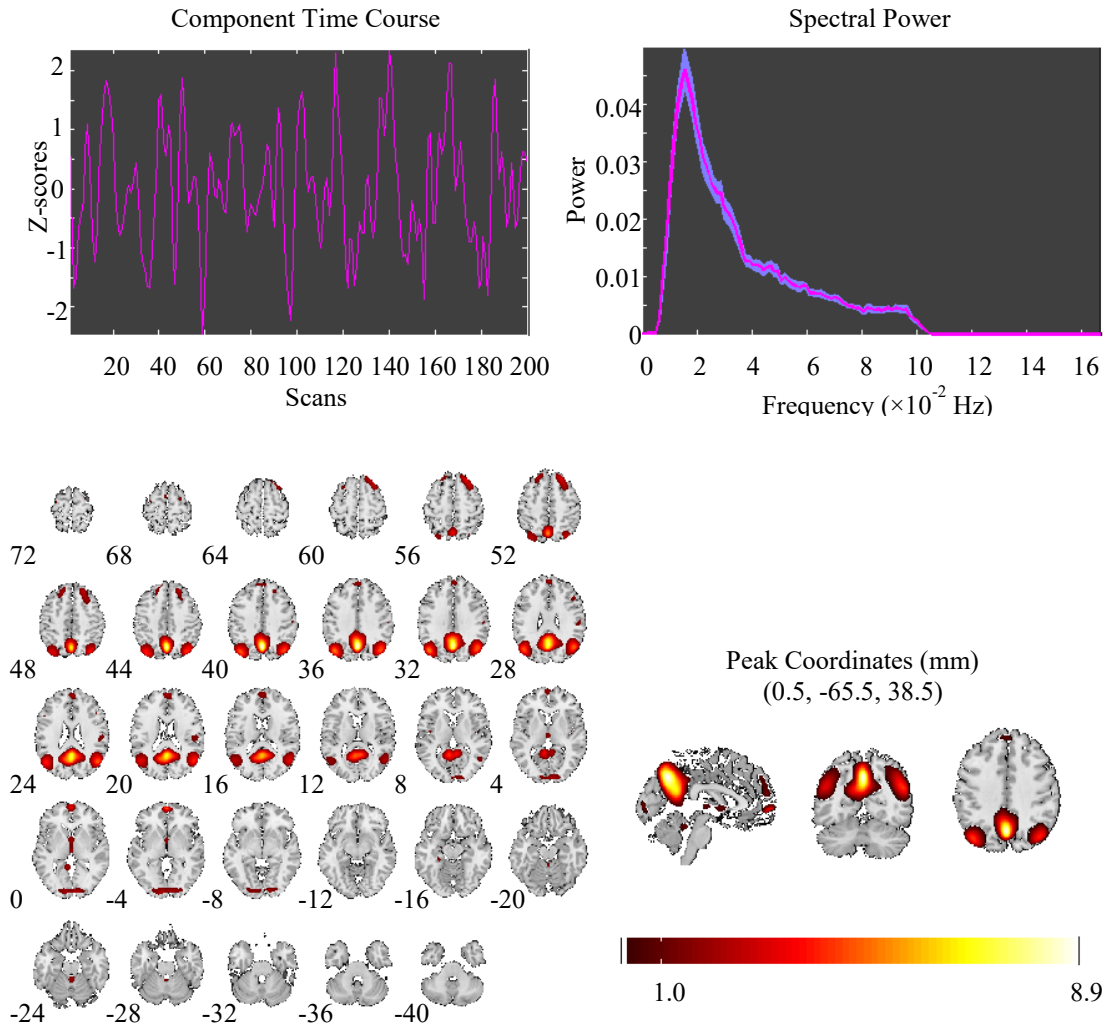


**Figure 1: Component 19: The Default Mode Network**

The upper left plot represents the average activity time course of all DMN voxels over the 10 minute resting state fMRI scan. The upper right plot displays the mean (pink) and standard error of mean (blue) spectral power across all participants and all DMN voxels. The lower left image shows DMN activity over 29 slices through the horizontal plane (group average). The lower right image displays the coordinates where peak activity was found in the DMN. Peak activity was localized in the PCC.

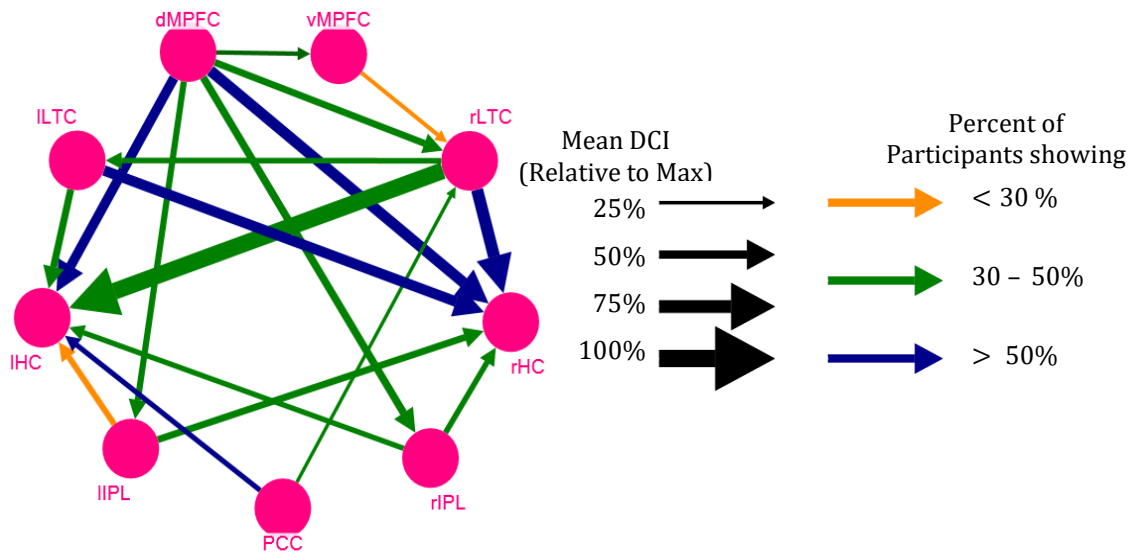


**Figure 2. Mean Differences of Causal Influence**

This figure displays the average DCI map across all participants, with a minimum threshold of 25% causal influence relative to the max. Each pink vertex represents one DMN ROI, as labeled. The arrows represent the directionality of the difference of causal influence from one ROI to another ROI. Arrow thickness defines the relative DCI, where the thickest arrow (from rLTC to IHC) is the max. Arrow color indicates whether less than 30% (orange), 30% - 50% (green), or greater than 50% (blue) of total participants exhibited a difference of causal influence. A maximum of 60% of total participants displayed a difference of significant causal influence between any two ROIs.

ROI to another as defined by  $F_{X \rightarrow Y|Z} - F_{X \rightarrow Y|Z}$ . Arrow thickness indicates the average DCI strength over all participants relative to the average DCI of the greatest strength. Arrow color indicates the percentage of total participants displaying a significant causal connection in the direction indicated.

The connections displayed in the mean network map (Figure 2) show stronger causal influence to both the IHC and rHPL relative to other ROIs. The strongest mean DCI is from the rLTC to the IHC (Figure 2, thick green arrow). The mean network map also shows that all DCIs exhibited by greater than 50% of participants are directed towards either the IHC or the rHPL (Figure 2, blue arrows). In addition, the IHC and rHPL receive

the five strongest influences, including all instances where the average DCI is greater than 50% relative to the max (Table 4). Further, with threshold of 25% mean DCI relative to the max, the lHC and rHC are the only ROIs that exhibit only efferent mean DCIs, while the dMPFC and PCC are the only ROI that only have afferent mean DCIs. It is of note that the PCC influences the lHC, and the dMPFC influences both the lHC and the rHC.

**Table 3: Average DCI Greater than 50% Relative to the Max**  
 This table lists the five strongest average DCIs, which are all directed towards the lHC or rHC.

<b>From</b>	<b>To</b>	<b>Mean DCI</b>
rLTC	lHC	100%
rLTC	rHC	76%
dMPFC	rHC	68%
lLTC	rHC	64%
dMPFC	lHC	62%

### 3.4. Cardiorespiratory Fitness Linearly Effects DMN Causal Influence

Linear regression modeling was used to predict the estimated DCI based on VO<sub>2</sub> max percentile. Figure 3 shows the models for which the VO<sub>2</sub> max percentile term was a significant predictor ( $p < 0.05$ ) of estimated DCI when physiological sex and handedness were held constant. For a list of all 36 linear regression models and p-values relating the nine ROIs, see Table 3. The models can be analyzed using the linear relationships. For example, if we take the significant effect of VO<sub>2</sub> max percentile on the DCI from the dMPFC to the lHC as represented by the red plot in figure 3D, we see the formula

$$y = 0.0075x + -0.1969,$$

where  $y$  is estimated DCI, and  $x$  is  $\text{VO}_2$  max percentile. This relationship exhibits the greatest slope, 0.0075 ( $r^2 = 0.59$ ), compared to other ROI pairs, indicating that it is most affected by changes in an individual's  $\text{VO}_2$  max percentile. Interestingly, Figure 3 also demonstrates that the DCI of each pair of effectively connected DMN regions may be positive or negative, depending on an individual's level of cardiorespiratory fitness. This implies that the DCI from one DMN region to another in a low-fit individual may be reversed in a high fitness individual. For example, a low-fit individual with a 10<sup>th</sup> percentile  $\text{VO}_2$  max would have a DCI from the IHC to the dMPFC of magnitude 0.16, while a high-fit individual with a 90<sup>th</sup> percentile  $\text{VO}_2$  max would have a DCI in the opposite direction from, the dMPFC to the IHC, of magnitude 0.52. The point in which the estimated DCI from the dMPFC to the IHC equals zero marks the point where the causal influence from the dMPFC to the IHC is equivalent to the causal influence from the IHC to the dMPFC.

Additionally, all linear regression models displayed in figure 3 show an increase in standard error of the model as  $\text{VO}_2$  max percentile increases, indicating a diminished model reliability as  $\text{VO}_2$  max percentile increases. This is likely due to the small number of participants clustered in the high  $\text{VO}_2$  max percentile range.

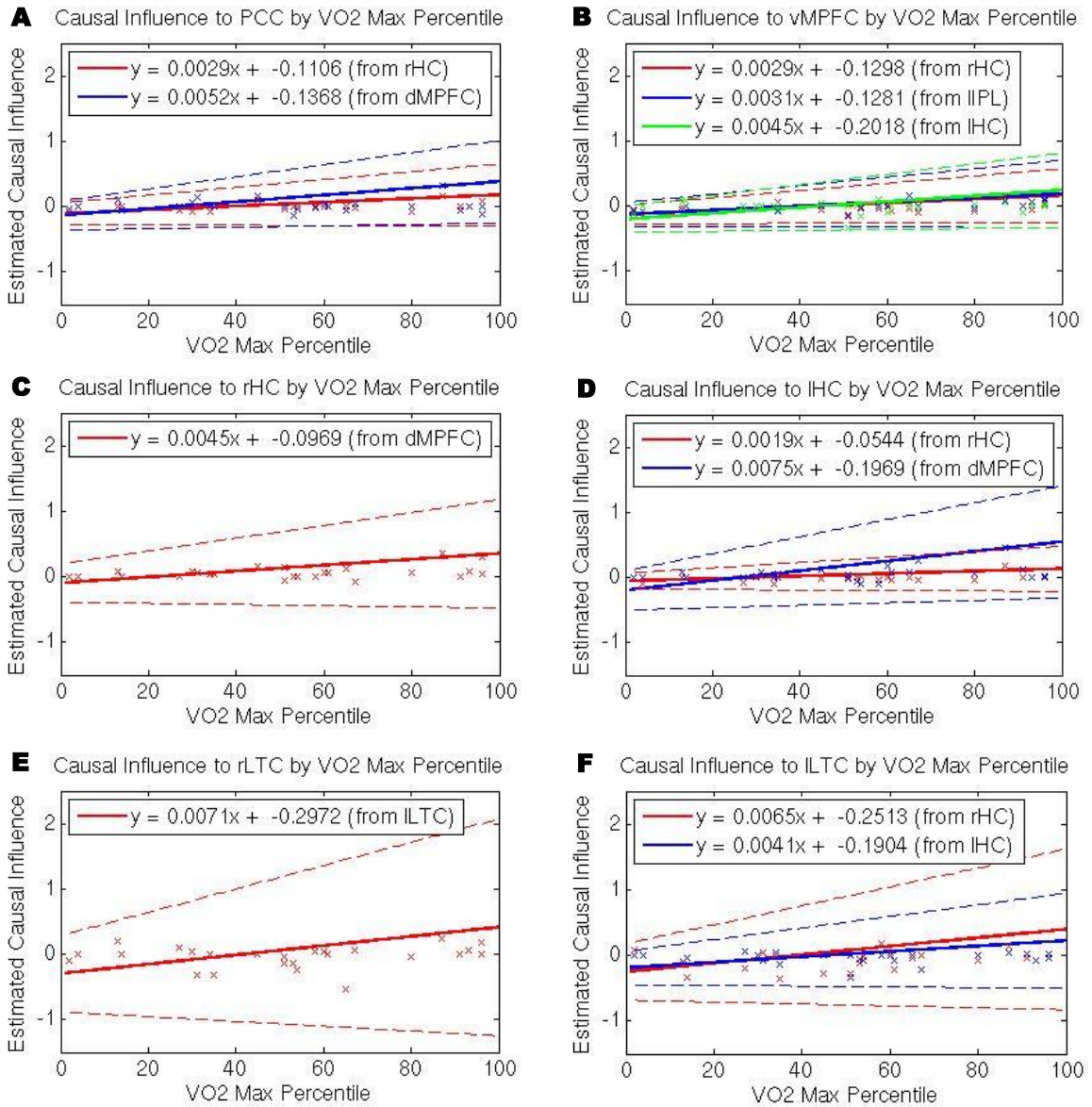


**Figure 3. Significant Linear Regression Model Plots**

This figure displays the linear regression model for the estimated DCI in which gender and handedness were controlled for and the VO<sub>2</sub> max percentile coefficient was statistically significant ( $p < 0.05$ ). The models are grouped by DCI to an ROI. Solid lines represent the linear regression model used to predict estimated DCI. The mathematical equation for each linear regression model is given in the legend, where, x represents the VO<sub>2</sub> max percentile, and y represents the estimated DCI. The dashed lines represent the standard error of the linear regression model in each figure of the same color. Each cross point represents the DCI between the two indicated ROIs for each individual participant. A positive estimated DCI indicates forward DCI according to the figure caption and legend. Negative estimated DCI indicates causality in the reverse direction indicated by the figure title and legend. An estimated DCI of zero indicates the point where the causal influence in both directions is equivalent. Figures A, B, C, D, E, and F display the linear regression model for DCI from the ROIs labeled by each legend to the PCC, vMPFC, rHC, IHC, rLTC, and ILTC, respectively.

**Table 4. All Linear Regression Models: Fitness Percentile by Causal Influence Between ROIs**

This table provides the linear regression model for each pair of ROIs, with controlled covariates (sex and handedness). Red p-values denote a statistically significant model (\*p < 0.05; \*\*p < 0.01; \*\*\*p < 0.001)

From ROI	To ROI	Controlled Linear Regression Model (y = DCI; x = VO2 Max %)	r <sup>2</sup>	VO2 Max Percentile p-Value
dMPFC	IHC	y = 0.0075x + -0.1969	0.5921	0.0004***
dMPFC	IPL	y = 0.0040x + -0.0973	0.1172	0.2617
dMPFC	ILTC	y = 0.0006x + 0.0227	0.2610	0.387
dMPFC	PCC	y = 0.0052x + -0.1368	0.6675	0.0001***
dMPFC	rHC	y = 0.0045x + -0.0969	0.4972	0.0250*
dMPFC	rIPL	y = 0.0043x + -0.1010	0.3520	0.0512
dMPFC	rLTC	y = 0.0056x + -0.1281	0.2982	0.0683
dMPFC	vMPFC	y = 0.0047x + -0.1606	0.3124	0.191
IHC	ILTC	y = 0.0041x + -0.1904	0.5091	0.0110*
IHC	PCC	y = 0.0006x + -0.0780	0.1538	0.7082
IHC	rLTC	y = 0.0013x + -0.1058	0.2139	0.5429
IHC	vMPFC	y = 0.0045x + -0.2018	0.7123	0.0004***
IPL	IHC	y = 0.0047x + -0.1630	0.4086	0.2016
IPL	ILTC	y = 0.0027x + -0.1090	0.3149	0.1941
IPL	PCC	y = 0.0010x + -0.0278	0.3464	0.5229
IPL	rHC	y = 0.0030x + -0.1025	0.4698	0.4082
IPL	rIPL	y = 0.0016x + -0.0323	0.2243	0.2968
IPL	rLTC	y = 0.0009x + -0.0115	0.2916	0.4845
IPL	vMPFC	y = 0.0031x + -0.1281	0.5198	0.0149*
ILTC	rLTC	y = 0.0071x + -0.2972	0.3317	0.0476*
ILTC	vMPFC	y = 0.0010x + -0.0352	0.1679	0.4379
PCC	ILTC	y = 0.0005x + -0.0345	0.2150	0.8291
PCC	rIPL	y = 0.0001x + -0.0107	0.2596	0.8229
rHC	IHC	y = 0.0019x + -0.0544	0.7029	0.0270*
rHC	ILTC	y = 0.0065x + -0.2513	0.4580	0.0156*
rHC	PCC	y = 0.0029x + -0.1106	0.4883	0.0084**
rHC	rLTC	y = 0.0034x + -0.1298	0.3116	0.1753
rHC	vMPFC	y = 0.0029x + -0.1298	0.6115	0.0018**
rIPL	IHC	y = 0.0008x + 0.0156	0.4101	0.6777
rIPL	ILTC	y = 0.0004x + -0.0142	0.1984	0.8391
rIPL	rHC	y = 0.0004x + 0.0260	0.3803	0.6956
rIPL	rLTC	y = 0.0005x + 0.0171	0.3550	0.4476
rIPL	vMPFC	y = 0.0020x + -0.1001	0.2563	0.1692
rLTC	PCC	y = 0.0018x + -0.1012	0.2549	0.2608
rLTC	vMPFC	y = 0.0009x + -0.0259	0.0879	0.5791
vMPFC	PCC	y = 0.0007x + -0.0022	0.1582	0.2832

#### 4. DISCUSSION

The primary purpose of this study was to investigate how cardiorespiratory fitness, as measured by VO<sub>2</sub> max percentile, may be used as to determine effective connectivity between the anatomical regions that define the DMN. The main components of this goal were (1) to identify the regions defining the DMN, (2) to determine the group level effective connectivity between the identified regions across participants, and (3) to define the relationship between effective connectivity of the DMN anatomical regions and cardiorespiratory fitness. This study was informed by a number of animal studies, which determined voluntary aerobic exercise is associated with increased AHN (Creer et al., 2010; Marlatt et al., 2012; Nokia et al., 2016; H. van Praag, Christie, et al., 1999; H. van Praag, Kempermann, et al., 1999), greater hippocampal vascularization (Creer et al., 2010), and improved hippocampal memory task performance (Clelland et al., 2009; Creer et al., 2010; Nokia et al., 2016; H. van Praag, Christie, et al., 1999) in young to middle aged adult mice. In support of previous studies, the results of this exploratory study found that the causal influence between the HC, MPFC, LTC, and PCC is significantly influenced by cardiorespiratory fitness, independent of sex and handedness, in a young human adult sample. We found that increased cardiorespiratory fitness significantly strengthened the causal influence from the HC bilaterally to the vMPFC and lLTC. In addition, cardiorespiratory fitness significantly affected the causal influence from the dMPFC to the HC, bilaterally, and to the PCC. Cardiorespiratory fitness also affected the causal influence from the rHC to the PCC, which is considered the primary hub of the DMN (R. L. Buckner et al., 2008).

#### **4.1. Default Mode Network Map of Effective Connectivity**

Figure 2 displays a DMN map describing the participant-wide average of the DCI between pairs of DMN regions that displayed significant causal influence. Recall that the average VO<sub>2</sub> max percentile over all participants is 52% ± 28%. This indicates that the cardiorespiratory fitness of the average sample population is similar to that of the average overall population of young adults (near 50%). Therefore, this network map should be a strong estimate of effective connectivity in the DMN of an average young adult.

The network map (Figure 2) suggests that the HC, bilaterally, is strongly co-activated with DMN regions, including the dMPFC, LTC, and PCC in sedentary young adults. This lends support to human studies that have established that the HC is strongly coupled to the DMN during memory retrieval (Bonnici et al., 2012; Huijbers et al., 2011; Kim, 2016). A number of studies have found that the HC and sub-regions of the prefrontal cortex are responsible for the storage and consciousness of episodic memories, respectively (Bonnici et al., 2012; Daselaar et al., 2008; Harand et al., 2012). Additionally, Daselaar and associates (2008) found that the MPFC, cingulate gyrus, and ventral prefrontal cortex are activated when healthy young adults “re-live” episodic memories, further supporting the involvement of the DMN in memory retrieval.

#### **4.2. Cardiorespiratory Fitness predicts DMN Effective Connectivity**

Moving on, the linear regression results confirm the predictive nature of cardiorespiratory fitness for eleven instances of effective connectivity between anatomical regions in the DMN. Note the number of effective connections predicted by

cardiorespiratory that involve the HC: eight of eleven of these instances involve either the rHC or the IHC, indicating that the effective connectivity of the HC is vastly affected by changes in cardiorespiratory fitness levels. Further, these connections are either with the MPFC, LTC, or PCC, which interact with the HC during memory tasks (Bonnici et al., 2012; Colcombe et al., 2006; Huijbers et al., 2011; Kim, 2016), as previously established.

These results may indirectly support rodent models that have established an association between voluntary aerobic exercise and AHN, increased vasculature in the hippocampus, and improved hippocampal memory task performance, as discussed above (Clelland et al., 2009; Creer et al., 2010; Marlatt et al., 2012; Nokia et al., 2016; H. van Praag, Christie, et al., 1999; Henriette van Praag et al., 2005; H. van Praag, Kempermann, et al., 1999). Although cardiorespiratory fitness is rarely used as an independent variable in rodent models, human studies have found that aerobic exercise leads to improved cardiorespiratory fitness (Hagberg et al., 1989; Kohrt et al., 1991). If this is also true of rodent models, the interaction between cardiorespiratory fitness and aerobic exercise may suggest that improved cardiorespiratory fitness is the underlying factor associated with the changes in AHN, vasculature, and hippocampal memory task performance in rodent models.

In conjunction with our results, this interaction has strong implications on human studies of aerobic exercise and memory retrieval. Investigators have concluded that aerobic exercise in healthy older adults resulted in an increase in grey matter in the prefrontal cortex (Colcombe et al., 2006) and the temporal cortex (Colcombe et al., 2006; Erickson et al., 2011). If aerobic exercise is associated with an increase in

cardiorespiratory fitness, we may also expect a corresponding change in effective connectivity between the prefrontal and temporal cortices (particularly the vMPFC, dMPFC, HC, and LTC), which may be explained by the increase in brain matter. This is further supported studies in older adults that have shown a positive correlation between cardiorespiratory fitness and hippocampal size (Erickson et al., 2009). These implications extend further, to hippocampal memory performance, which has been positively correlated with the size of the HC (Erickson et al., 2011).

Moreover, these results build on human studies that have measured cardiorespiratory fitness directly, showing that cardiorespiratory fitness may be positively correlated with hippocampal memory performance in young adults (Baym et al., 2014; Pontifex et al., 2014). Together with the findings of previous animal models and human studies, our results lend support to the idea that as AHN is enhanced by improving cardiorespiratory fitness, via aerobic exercise, the effective connectivity between the HC and the MRFC, LTC and PCC may be enhanced. Such enhancements in the flow of information within the DMN may be responsible for improved hippocampal memory performance after aerobic exercise training.

#### **4.3. Implications for Preclinical Alzheimer's Disease**

Investigators have previously associated changes in the DMN with the development of AD (Greicius et al., 2004; Hafkemeijer et al., 2012; Koch et al., 2012; Mevel et al., 2011; Miao et al., 2011; Rombouts et al., 2005; Sorg et al., 2007; Wang et al., 2013). The earliest findings noted diminished glucose metabolism in the PCC, IPL,

and LTC with the progression of AD (R. L. Buckner et al., 2008; Greicius et al., 2004; Kumar et al., 1991). Additional changes to the DMN include diminished functional connectivity (Greicius et al., 2004; Mevel et al., 2011; Rombouts et al., 2005), and altered effective connectivity between anatomical structures (Miao et al., 2011). Moreover, it is well established that the HC begins to atrophy during the early stages of AD (Randy L. Buckner et al., 2005; Mevel et al., 2011; Sorg et al., 2007; Wang et al., 2013). During the preclinical stage of AD there may be very subtle changes, such as subjective cognitive problems; however, there are no objective cognitive impairments or obvious atrophy that would not be considered normal for older adults.

Investigators have examined how cardiorespiratory fitness may be used to estimate factors that are known to change in preclinical and early clinical AD. One study revealed a positive correlation between cardiorespiratory fitness and functional connectivity within the DMN in older adults (Voss et al., 2015). Another study demonstrated that greater cardiorespiratory fitness may be associated with less atrophy of the HC as the brain ages in older adults with early clinical AD (Vidoni et al., 2012). This agrees with models that have revealed how cardiorespiratory fitness is positively correlated with hippocampal volume in older adults (Erickson et al., 2009, 2011). Interestingly, Honea and colleagues (2009) noticed that the volume of the medial temporal lobe, and parietal cortex was positively correlated with cardiorespiratory fitness in older adults with early clinical AD, but not in healthy older adults. This indicates that a correlation between cardiorespiratory fitness and hippocampal volume without abnormal cognitive impairments may be a sign of preclinical AD.

A report by Miao and associates (2011) showed a severely modified pattern of effective connectivity between DMN regions in older adults with AD compared to that of healthy older adults. In showing changes in effective connectivity with AD, the work by Miao and associates (2011) strongly supports how our work acts as a proof of concept, which establishes that resting state fMRI may be used in conjunction with effective connectivity analysis, using CGCA, to examine subtle changes in causal influence, adds to the body of literature demonstrating that resting state fMRI may be used to examine how neurological pathologies arise during the progression of preclinical and early clinical AD. Additional work is needed to determine if these methods may be used to analyze neuronal changes during the preclinical stage of AD, as well as during preclinical AD interventions, such as aerobic exercise.

#### **4.4. Limitations**

When analyzing our data, it is important to consider the limitations of our results. First, in using complex, data-driven, linear modeling methods, such as GICA and CGCA, larger data sets create stronger models. Our results demonstrated a number of trends, with few significant models. A larger sample size may yield further significant predictive information.

Additionally, the resting state scan was performed directly following a delayed match to sample task involving hippocampal memory. Although the participants were instructed to relax and not think of anything in particular, it is possible that their attention was directed at the previous task or another task entirely. Therefore, the data presented

here may be associated with a form of implicit retrieval or consolidation. This type of interference was not controlled, and could not be eliminated definitively.

Moreover, of the 25 ICs extracted during GICA, one was selected (Fig. 1) to represent the DMN as in other studies (Greicius et al., 2007; Koch et al., 2012). However, other studies have grouped more than one IC to represent the DMN (Damoiseaux et al., 2006; Rombouts et al., 2009). Although our method of visual inspection and DMN template correlation did not reveal another IC to be a part of the DMN, we cannot eliminate the possibility of missing data from another IC with certainty.

Finally, the poor temporal resolution of fMRI data can be an obstacle when using CGCA (Deshpande & Hu, 2012; Deshpande et al., 2011; Zhou et al., 2009). The temporal resolution for fMRI is typically in the range of 1 to 3 seconds. If the causal events being investigated occur at a higher temporal resolution than can be recorded, data analysis may misinterpret causal relationships due to under-sampling of the data (Deshpande et al., 2011). However, compared to task-evoked BOLD activity, resting state spontaneous activity occurs at a low frequency range: 0.01Hz – 0.1Hz (Biswal et al., 2010; Damoiseaux et al., 2006; Rosazza & Minati, 2011). Therefore, we can assume that resting state fMRI is not affected by poor temporal resolution of fMRI instrumentation (Deshpande et al., 2011).

#### **4.5. Future Directions**

Further studies are needed to determine how cardiorespiratory fitness may act as a predictor of effective connectivity in the DMN in populations of healthy older adults, and

older adults with preclinical and early clinical AD. Additionally, future work will be required to examine how effective connectivity in the DMN of older adults with preclinical AD responds to aerobic exercise intervention.

#### **4.6. Conclusion**

This work extends previous animal models on adult neurogenesis and hippocampal memory by suggesting aerobic exercise may strengthen memory performance by improving cardiorespiratory fitness, therefore enhancing effective connections between the hippocampus and other brain areas important for memory performance, such as the vMPFC, dMPFC, PCC, and LTC. Further, this has implications as to potential prevention and treatments of neurological pathologies associated with preclinical AD, for which individuals experience diminished effective connectivity in the DMN. Additional research is required to determine if improving cardiorespiratory fitness can be used to counteract neurological pathologies associated with preclinical AD by improving DMN connectivity.

## 5. REFERENCES

- Aging, N. I. on. (2014, July 1). Introduction [Text]. Retrieved December 9, 2015, from <https://www.nia.nih.gov/alzheimers/publication/2013-2014-alzheimers-disease-progress-report/introduction>
- American College of Sports Medicine, Thompson, W. R., Gordon, N. F., & Pescatello, L. S. (2010). *ACSM's guidelines for exercise testing and prescription*. Philadelphia: Wolters Kluwer/Lippincott Williams & Wilkins.
- Andrews-Hanna, J. R. (2012). The Brain's Default Network and its Adaptive Role in Internal Mentation. *The Neuroscientist : A Review Journal Bringing Neurobiology, Neurology and Psychiatry*, *18*(3), 251–270. <http://doi.org/10.1177/1073858411403316>
- Barnett, L., & Seth, A. K. (2014). The MVGC multivariate Granger causality toolbox: A new approach to Granger-causal inference. *Journal of Neuroscience Methods*, *223*, 50–68. <http://doi.org/10.1016/j.jneumeth.2013.10.018>
- Baym, C. L., Khan, N. A., Pence, A., Raine, L. B., Hillman, C. H., & Cohen, N. J. (2014). Aerobic fitness predicts relational memory but not item memory performance in healthy young adults. *Journal of Cognitive Neuroscience*, *26*(11), 2645–2652. [http://doi.org/10.1162/jocn\\_a\\_00667](http://doi.org/10.1162/jocn_a_00667)
- Beckmann, C. F., DeLuca, M., Devlin, J. T., & Smith, S. M. (2005). Investigations into resting-state connectivity using independent component analysis. *Philosophical Transactions of the Royal Society B: Biological Sciences*, *360*(1457), 1001–1013. <http://doi.org/10.1098/rstb.2005.1634>
- Binder, J. R., Frost, J. A., Hammeke, T. A., Bellgowan, P. S., Rao, S. M., & Cox, R. W. (1999). Conceptual processing during the conscious resting state. A functional MRI study. *Journal of Cognitive Neuroscience*, *11*(1), 80–95.
- Biswal, B. B., Mennes, M., Zuo, X.-N., Gohel, S., Kelly, C., Smith, S. M., ... Milham, M. P. (2010). Toward discovery science of human brain function. *Proceedings of the National Academy of Sciences*, *107*(10), 4734–4739. <http://doi.org/10.1073/pnas.0911855107>
- Bonnici, H. M., Chadwick, M. J., Lutti, A., Hassabis, D., Weiskopf, N., & Maguire, E. A. (2012). Detecting Representations of Recent and Remote Autobiographical Memories in vmPFC and Hippocampus. *Journal of Neuroscience*, *32*(47), 16982–16991. <http://doi.org/10.1523/JNEUROSCI.2475-12.2012>

- Bressler, S. L., & Seth, A. K. (2011). Wiener–Granger Causality: A well established methodology. *NeuroImage*, *58*(2), 323–329.  
<http://doi.org/10.1016/j.neuroimage.2010.02.059>
- Brett, M., Anton, J. L., Valabregue, R., & Poline, J. B. (2002). MarsBaR Documentation.
- Buckner, R. L., Andrews-Hanna, J. R., & Schacter, D. L. (2008). The Brain’s Default Network: Anatomy, Function, and Relevance to Disease. *Annals of the New York Academy of Sciences*, *1124*(1), 1–38. <http://doi.org/10.1196/annals.1440.011>
- Buckner, R. L., Snyder, A. Z., Shannon, B. J., LaRossa, G., Sachs, R., Fotenos, A. F., ... Mintun, M. A. (2005). Molecular, structural, and functional characterization of Alzheimer’s disease: evidence for a relationship between default activity, amyloid, and memory. *The Journal of Neuroscience: The Official Journal of the Society for Neuroscience*, *25*(34), 7709–7717.  
<http://doi.org/10.1523/JNEUROSCI.2177-05.2005>
- Burdette. (2010). Using network science to evaluate exercise-associated brain changes in older adults. *Frontiers in Aging Neuroscience*.  
<http://doi.org/10.3389/fnagi.2010.00023>
- CDC - Healthy Brain Initiative: Alzheimer’s Disease - Aging. (2015, March 5). [Text]. Retrieved December 9, 2015, from  
<http://www.cdc.gov/aging/aginginfo/alzheimers.htm>
- Clelland, C. D., Choi, M., Romberg, C., Clemenson, G. D., Fagniere, A., Tyers, P., ... Bussey, T. J. (2009). A functional role for adult hippocampal neurogenesis in spatial pattern separation. *Science (New York, N.Y.)*, *325*(5937), 210–213.  
<http://doi.org/10.1126/science.1173215>
- Colcombe, S. J., Erickson, K. I., Scalf, P. E., Kim, J. S., Prakash, R., McAuley, E., ... Kramer, A. F. (2006). Aerobic exercise training increases brain volume in aging humans. *The Journals of Gerontology. Series A, Biological Sciences and Medical Sciences*, *61*(11), 1166–1170.
- Cole. (2010). Advances and pitfalls in the analysis and interpretation of resting-state FMRI data. *Frontiers in Systems Neuroscience*.  
<http://doi.org/10.3389/fnsys.2010.00008>
- Cooper, C. B., & Storer, T. W. (2001). *Exercise Testing and Interpretation: A Practical Approach*. Cambridge University Press.
- Creer, D. J., Romberg, C., Saksida, L. M., Praag, H. van, & Bussey, T. J. (2010). Running enhances spatial pattern separation in mice. *Proceedings of the National*

*Academy of Sciences*, 107(5), 2367–2372.  
<http://doi.org/10.1073/pnas.0911725107>

- Damoiseaux, J. S., Rombouts, S., Barkhof, F., Scheltens, P., Stam, C. J., Smith, S. M., & Beckmann, C. F. (2006). Consistent resting-state networks across healthy subjects. *Proceedings of the National Academy of Sciences*, 103(37), 13848–13853.
- Daselaar, S. M., Rice, H. J., Greenberg, D. L., Cabeza, R., LaBar, K. S., & Rubin, D. C. (2008). The Spatiotemporal Dynamics of Autobiographical Memory: Neural Correlates of Recall, Emotional Intensity, and Reliving. *Cerebral Cortex*, 18(1), 217–229. <http://doi.org/10.1093/cercor/bhm048>
- De Luca, M., Beckmann, C. F., De Stefano, N., Matthews, P. M., & Smith, S. M. (2006). fMRI resting state networks define distinct modes of long-distance interactions in the human brain. *NeuroImage*, 29(4), 1359–1367. <http://doi.org/10.1016/j.neuroimage.2005.08.035>
- Deshpande, G., & Hu, X. (2012). Investigating Effective Brain Connectivity from fMRI Data: Past Findings and Current Issues with Reference to Granger Causality Analysis. *Brain Connectivity*, 2(5), 235–245. <http://doi.org/10.1089/brain.2012.0091>
- Deshpande, G., LaConte, S., James, G. A., Peltier, S., & Hu, X. (2009). Multivariate Granger causality analysis of fMRI data. *Human Brain Mapping*, 30(4), 1361–1373. <http://doi.org/10.1002/hbm.20606>
- Deshpande, G., Santhanam, P., & Hu, X. (2011). Instantaneous and causal connectivity in resting state brain networks derived from functional MRI data. *NeuroImage*, 54(2), 1043–1052. <http://doi.org/10.1016/j.neuroimage.2010.09.024>
- Eichenbaum, H. (2000). A cortical–hippocampal system for declarative memory. *Nature Reviews Neuroscience*, 1(1), 41–50. <http://doi.org/10.1038/35036213>
- Erickson, K. I., Prakash, R. S., Voss, M. W., Chaddock, L., Hu, L., Morris, K. S., ... Kramer, A. F. (2009). Aerobic Fitness is Associated With Hippocampal Volume in Elderly Humans. *Hippocampus*, 19(10), 1030–1039. <http://doi.org/10.1002/hipo.20547>
- Erickson, K. I., Voss, M. W., Prakash, R. S., Basak, C., Szabo, A., Chaddock, L., ... Kramer, A. F. (2011). Exercise training increases size of hippocampus and improves memory. *Proceedings of the National Academy of Sciences of the United States of America*, 108(7), 3017–3022. <http://doi.org/10.1073/pnas.1015950108>

- Eye, A. von, Wiedermann, W., & Mun, E.-Y. (2013). Granger Causality—Statistical Analysis Under a Configural Perspective. *Integrative Psychological and Behavioral Science*, 48(1), 79–99. <http://doi.org/10.1007/s12124-013-9243-1>
- Faro, S. H., & Mohamed, F. B. (Eds.). (2010). *BOLD fMRI*. New York, NY: Springer New York. Retrieved from <http://link.springer.com/10.1007/978-1-4419-1329-6>
- Fox, M. D., Snyder, A. Z., Vincent, J. L., Corbetta, M., Van Essen, D. C., & Raichle, M. E. (2005). The human brain is intrinsically organized into dynamic, anticorrelated functional networks. *Proceedings of the National Academy of Sciences of the United States of America*, 102(27), 9673–9678.
- Franco, A. R., Pritchard, A., Calhoun, V. D., & Mayer, A. R. (2009). Interrater and intermethod reliability of default mode network selection. *Human Brain Mapping*, 30(7), 2293–2303. <http://doi.org/10.1002/hbm.20668>
- Friston, K. J. (2011). Functional and Effective Connectivity: A Review. *Brain Connectivity*, 1(1), 13–36. <http://doi.org/10.1089/brain.2011.0008>
- Friston, K. J., & others. (1994). Functional and effective connectivity in neuroimaging: a synthesis. *Human Brain Mapping*, 2(1-2), 56–78.
- Geweke, J. F. (1984). Measures of Conditional Linear Dependence and Feedback Between Time Series. *Journal of the American Statistical Association*, 79(388), 907–915. <http://doi.org/10.2307/2288723>
- Gilbert, S. J., Dumontheil, I., Simons, J. S., Frith, C. D., & Burgess, P. W. (2007). Comment on “Wandering Minds: The Default Network and Stimulus-Independent Thought.” *Science*, 317(5834), 43b–43b. <http://doi.org/10.1126/science.1140801>
- Goebel, R., Roebroeck, A., Kim, D.-S., & Formisano, E. (2003). Investigating directed cortical interactions in time-resolved fMRI data using vector autoregressive modeling and Granger causality mapping. *Magnetic Resonance Imaging*, 21(10), 1251–1261.
- Gore, J. C. (2003). Principles and practice of functional MRI of the human brain. *Journal of Clinical Investigation*, 112(1), 4–9. <http://doi.org/10.1172/JCI200319010>
- Granger, C. W. J. (1969). Investigating Causal Relations by Econometric Models and Cross-spectral Methods. *Econometrica*, 37(3), 424–438. <http://doi.org/10.2307/1912791>
- Greicius, M. D., Flores, B. H., Menon, V., Glover, G. H., Solvason, H. B., Kenna, H., ... Schatzberg, A. F. (2007). Resting-State Functional Connectivity in Major Depression: Abnormally Increased Contributions from Subgenual Cingulate

Cortex and Thalamus. *Biological Psychiatry*, 62(5), 429–437.  
<http://doi.org/10.1016/j.biopsych.2006.09.020>

Greicius, M. D., Srivastava, G., Reiss, A. L., & Menon, V. (2004). Default-mode network activity distinguishes Alzheimer's disease from healthy aging: evidence from functional MRI. *Proceedings of the National Academy of Sciences of the United States of America*, 101(13), 4637–4642.

Griffin, É. W., Mullally, S., Foley, C., Warmington, S. A., O'Mara, S. M., & Kelly, A. M. (2011). Aerobic exercise improves hippocampal function and increases BDNF in the serum of young adult males. *Physiology & Behavior*, 104(5), 934–941.  
<http://doi.org/10.1016/j.physbeh.2011.06.005>

Hafkemeijer, A., van der Grond, J., & Rombouts, S. A. R. B. (2012). Imaging the default mode network in aging and dementia. *Biochimica et Biophysica Acta (BBA) - Molecular Basis of Disease*, 1822(3), 431–441.  
<http://doi.org/10.1016/j.bbadis.2011.07.008>

Hagberg, J. M., Graves, J. E., Limacher, M., Woods, D. R., Leggett, S. H., Cononie, C., ... Pollock, M. L. (1989). Cardiovascular responses of 70- to 79-yr-old men and women to exercise training. *Journal of Applied Physiology (Bethesda, Md.: 1985)*, 66(6), 2589–2594.

Hahn, B., Ross, T. J., & Stein, E. A. (2007). Cingulate activation increases dynamically with response speed under stimulus unpredictability. *Cerebral Cortex (New York, N.Y.: 1991)*, 17(7), 1664–1671. <http://doi.org/10.1093/cercor/bhl075>

Harand, C., Bertran, F., Joie, R. L., Landeau, B., Mézenge, F., Desgranges, B., ... Rauchs, G. (2012). The Hippocampus Remains Activated over the Long Term for the Retrieval of Truly Episodic Memories. *PLOS ONE*, 7(8), e43495.  
<http://doi.org/10.1371/journal.pone.0043495>

Hebert, L. E., Weuve, J., Scherr, P. A., & Evans, D. A. (2013). Alzheimer disease in the United States (2010-2050) estimated using the 2010 census. *Neurology*, 80(19), 1778–1783. <http://doi.org/10.1212/WNL.0b013e31828726f5>

Himberg, J., & Hyvärinen, A. (2003). Icasto: software for investigating the reliability of ICA estimates by clustering and visualization. In *Neural Networks for Signal Processing, 2003. NNSP'03. 2003 IEEE 13th Workshop on* (pp. 259–268). IEEE. Retrieved from [http://ieeexplore.ieee.org/xpls/abs\\_all.jsp?arnumber=1318025](http://ieeexplore.ieee.org/xpls/abs_all.jsp?arnumber=1318025)

Honea, R., Thomas, G. P., Harsha, A., Anderson, H. S., Donnelly, J. E., Brooks, W. M., & Burns, J. M. (2009). Cardiorespiratory fitness and preserved medial temporal lobe volume in Alzheimer's Disease. *Alzheimer Disease and Associated Disorders*, 23(3), 188–197. <http://doi.org/10.1097/WAD.0b013e31819cb8a2>

- Horwitz, B. (2003). The elusive concept of brain connectivity. *NeuroImage*, *19*(2), 466–470. [http://doi.org/10.1016/S1053-8119\(03\)00112-5](http://doi.org/10.1016/S1053-8119(03)00112-5)
- Huang, E. J., & Reichardt, L. F. (2001). Neurotrophins: Roles in Neuronal Development and Function. *Annual Review of Neuroscience*, *24*, 677–736. <http://doi.org/10.1146/annurev.neuro.24.1.677>
- Huijbers, W., Pennartz, C. M. A., Cabeza, R., & Daselaar, S. M. (2011). The hippocampus is coupled with the default network during memory retrieval but not during memory encoding. *PloS One*, *6*(4), e17463. <http://doi.org/10.1371/journal.pone.0017463>
- Ingvar, D. H. (1979). “Hyperfrontal” distribution of the cerebral grey matter flow in resting wakefulness; on the functional anatomy of the conscious state. *Acta Neurologica Scandinavica*, *60*(1), 12–25.
- Ingvar, D. H., & Franzén, G. (1974). Abnormalities of Cerebral Blood Flow Distribution in Patients with Chronic Schizophrenia. *Acta Psychiatrica Scandinavica*, *50*(4), 425–462. <http://doi.org/10.1111/j.1600-0447.1974.tb09707.x>
- Joel, S. E., Caffo, B. S., van Zijl, P. C., & Pekar, J. J. (2011). On the relationship between seed-based and ICA-based measures of functional connectivity. *Magnetic Resonance in Medicine : Official Journal of the Society of Magnetic Resonance in Medicine / Society of Magnetic Resonance in Medicine*, *66*(3), 644–657. <http://doi.org/10.1002/mrm.22818>
- Jones, D. T., Machulda, M. M., Vemuri, P., McDade, E. M., Zeng, G., Senjem, M. L., ... Jack, C. R. (2011). Age-related changes in the default mode network are more advanced in Alzheimer disease. *Neurology*, *77*(16), 1524–1531. <http://doi.org/10.1212/WNL.0b013e318233b33d>
- Kelly, R. E., Alexopoulos, G. S., Wang, Z., Gunning, F. M., Murphy, C. F., Morimoto, S. S., ... Hoptman, M. J. (2010). Visual inspection of independent components: Defining a procedure for artifact removal from fMRI data. *Journal of Neuroscience Methods*, *189*(2), 233–245. <http://doi.org/10.1016/j.jneumeth.2010.03.028>
- Kim, H. (2015). Encoding and retrieval along the long axis of the hippocampus and their relationships with dorsal attention and default mode networks: The HERNET model. *Hippocampus*, *25*(4), 500–510. <http://doi.org/10.1002/hipo.22387>
- Kim, H. (2016). Default network activation during episodic and semantic memory retrieval: A selective meta-analytic comparison. *Neuropsychologia*, *80*, 35–46. <http://doi.org/10.1016/j.neuropsychologia.2015.11.006>

- Koch, W., Teipel, S., Mueller, S., Benninghoff, J., Wagner, M., Bokde, A. L. W., ... Meindl, T. (2012). Diagnostic power of default mode network resting state fMRI in the detection of Alzheimer's disease. *Neurobiology of Aging*, 33(3), 466–478. <http://doi.org/10.1016/j.neurobiolaging.2010.04.013>
- Kohrt, W. M., Malley, M. T., Coggan, A. R., Spina, R. J., Ogawa, T., Ehsani, A. A., ... Holloszy, J. O. (1991). Effects of gender, age, and fitness level on response of VO2max to training in 60-71 yr olds. *Journal of Applied Physiology*, 71(5), 2004–2011.
- Kumar, A., Schapiro, M. B., Grady, C., Haxby, J. V., Wagner, E., Salerno, J. A., ... Rapoport, S. I. (1991). High-resolution PET studies in Alzheimer's disease. *Neuropsychopharmacology: Official Publication of the American College of Neuropsychopharmacology*, 4(1), 35–46.
- Leopold, D. A., Murayama, Y., & Logothetis, N. K. (2003). Very slow activity fluctuations in monkey visual cortex: implications for functional brain imaging. *Cerebral Cortex (New York, N.Y.: 1991)*, 13(4), 422–433.
- Liao, W., Mantini, D., Zhang, Z., Pan, Z., Ding, J., Gong, Q., ... Chen, H. (2009). Evaluating the effective connectivity of resting state networks using conditional Granger causality. *Biological Cybernetics*, 102(1), 57–69. <http://doi.org/10.1007/s00422-009-0350-5>
- Li, R., Zhu, X., Yin, S., Niu, Y., Zheng, Z., Huang, X., ... Li, J. (2014). Multimodal intervention in older adults improves resting-state functional connectivity between the medial prefrontal cortex and medial temporal lobe†. *Frontiers in Aging Neuroscience*, 6. <http://doi.org/10.3389/fnagi.2014.00039>
- Logothetis, N. K. (2003). The Underpinnings of the BOLD Functional Magnetic Resonance Imaging Signal. *The Journal of Neuroscience*, 23(10), 3963–3971.
- Maass, A., Düzel, S., Goerke, M., Becke, A., Sobieray, U., Neumann, K., ... Düzel, E. (2015). Vascular hippocampal plasticity after aerobic exercise in older adults. *Molecular Psychiatry*, 20(5), 585–593. <http://doi.org/10.1038/mp.2014.114>
- Mantini, D., & Vanduffel, W. (2013). Emerging Roles of the Brain's Default Network. *The Neuroscientist*, 19(1), 76–87. <http://doi.org/10.1177/1073858412446202>
- Marlatt, M. W., Potter, M. C., Lucassen, P. J., & van Praag, H. (2012). Running throughout middle-age improves memory function, hippocampal neurogenesis, and BDNF levels in female C57BL/6J mice. *Developmental Neurobiology*, 72(6), 943–952. <http://doi.org/10.1002/dneu.22009>

- Mason, M. F., Norton, M. I., Van Horn, J. D., Wegner, D. M., Grafton, S. T., & Macrae, C. N. (2007). Wandering minds: the default network and stimulus-independent thought. *Science (New York, N.Y.)*, *315*(5810), 393–395. <http://doi.org/10.1126/science.1131295>
- Mazoyer, B., Zago, L., Mellet, E., Bricogne, S., Etard, O., Houdé, O., ... Tzourio-Mazoyer, N. (2001). Cortical networks for working memory and executive functions sustain the conscious resting state in man. *Brain Research Bulletin*, *54*(3), 287–298. [http://doi.org/10.1016/S0361-9230\(00\)00437-8](http://doi.org/10.1016/S0361-9230(00)00437-8)
- Mevel, K., Ch&#233, Telat, G., l, Eustache, F., Desgranges, B., & atrice. (2011). The Default Mode Network in Healthy Aging and Alzheimer’s Disease. *International Journal of Alzheimer’s Disease*, *2011*, e535816. <http://doi.org/10.4061/2011/535816>
- Miao, X., Wu, X., Li, R., Chen, K., & Yao, L. (2011). Altered Connectivity Pattern of Hubs in Default-Mode Network with Alzheimer’s Disease: An Granger Causality Modeling Approach. *PLoS ONE*, *6*(10), e25546. <http://doi.org/10.1371/journal.pone.0025546>
- Nokia, M. S., Lensu, S., Ahtiainen, J. P., Johansson, P. P., Koch, L. G., Britton, S. L., & Kainulainen, H. (2016). Physical exercise increases adult hippocampal neurogenesis in male rats provided it is aerobic and sustained. *The Journal of Physiology*, n/a–n/a. <http://doi.org/10.1113/JP271552>
- Pereira, A. C., Huddleston, D. E., Brickman, A. M., Sosunov, A. A., Hen, R., McKhann, G. M., ... Small, S. A. (2007). An in vivo correlate of exercise-induced neurogenesis in the adult dentate gyrus. *Proceedings of the National Academy of Sciences*, *104*(13), 5638–5643. <http://doi.org/10.1073/pnas.0611721104>
- Pontifex, M. B., Parks, A. C., O’Neil, P. C., Egner, A. R., Warning, J. T., Pfeiffer, K. A., & Fenn, K. M. (2014). Poorer aerobic fitness relates to reduced integrity of multiple memory systems. *Cognitive, Affective & Behavioral Neuroscience*, *14*(3), 1132–1141. <http://doi.org/10.3758/s13415-014-0265-z>
- Rachakonda, S., Egolf, E., Correa, N., & Calhoun, V. (2007). Group ICA of fMRI toolbox (GIFT) manual. *Dostupné Z: Http://www. Nitrc. Org/docman/view.php/55/295/v1. 3d\_GIFTManual. Pdf [cit. 2011-11-5]*. Retrieved from [http://mialab.mrn.org/software/gift/docs/v1.3i\\_GIFTManual.pdf](http://mialab.mrn.org/software/gift/docs/v1.3i_GIFTManual.pdf)
- Raichle, M. E. (2015). The Brain’s Default Mode Network. *Annual Review of Neuroscience*, *38*(1), 433–447. <http://doi.org/10.1146/annurev-neuro-071013-014030>

- Roebroeck, A., Formisano, E., & Goebel, R. (2005). Mapping directed influence over the brain using Granger causality and fMRI. *NeuroImage*, *25*(1), 230–242. <http://doi.org/10.1016/j.neuroimage.2004.11.017>
- Roebroeck, A., Formisano, E., & Goebel, R. (2011). The identification of interacting networks in the brain using fMRI: Model selection, causality and deconvolution. *NeuroImage*, *58*(2), 296–302. <http://doi.org/10.1016/j.neuroimage.2009.09.036>
- Rombouts, S. A. R. B., Barkhof, F., Goekoop, R., Stam, C. J., & Scheltens, P. (2005). Altered resting state networks in mild cognitive impairment and mild Alzheimer's disease: An fMRI study. *Human Brain Mapping*, *26*(4), 231–239. <http://doi.org/10.1002/hbm.20160>
- Rombouts, S. A. R. B., Damoiseaux, J. S., Goekoop, R., Barkhof, F., Scheltens, P., Smith, S. M., & Beckmann, C. F. (2009). Model-free group analysis shows altered BOLD FMRI networks in dementia. *Human Brain Mapping*, *30*(1), 256–266. <http://doi.org/10.1002/hbm.20505>
- Rosazza, C., & Minati, L. (2011). Resting-state brain networks: literature review and clinical applications. *Neurological Sciences*, *32*(5), 773–785. <http://doi.org/10.1007/s10072-011-0636-y>
- Shmuel, A., & Leopold, D. A. (2008). Neuronal correlates of spontaneous fluctuations in fMRI signals in monkey visual cortex: Implications for functional connectivity at rest. *Human Brain Mapping*, *29*(7), 751–761. <http://doi.org/10.1002/hbm.20580>
- Shors, T. J., Miesegaes, G., Beylin, A., Zhao, M., Rydel, T., & Gould, E. (2001). Neurogenesis in the adult is involved in the formation of trace memories. *Nature*, *410*(6826), 372–376. <http://doi.org/10.1038/35066584>
- Shulman, G. L., Fiez, J. A., Corbetta, M., Buckner, R. L., Miezin, F. M., Raichle, M. E., & Petersen, S. E. (1997). Common Blood Flow Changes across Visual Tasks: II. Decreases in Cerebral Cortex. *Journal of Cognitive Neuroscience*, *9*(5), 648–663. <http://doi.org/10.1162/jocn.1997.9.5.648>
- Sorg, C., Riedl, V., Mühlau, M., Calhoun, V. D., Eichele, T., Läer, L., ... others. (2007). Selective changes of resting-state networks in individuals at risk for Alzheimer's disease. *Proceedings of the National Academy of Sciences*, *104*(47), 18760–18765.
- Sporns, O. (2007). Brain connectivity. *Scholarpedia*, *2*(10). <http://doi.org/10.4249/scholarpedia.4695>
- Tang, W., Bressler, S. L., Sylvester, C. M., Shulman, G. L., & Corbetta, M. (2012). Measuring Granger Causality between Cortical Regions from Voxelwise fMRI

BOLD Signals with LASSO. *PLoS Computational Biology*, 8(5), e1002513.  
<http://doi.org/10.1371/journal.pcbi.1002513>

Vanhaudenhuyse, A., Noirhomme, Q., Tshibanda, L. J.-F., Bruno, M.-A., Boveroux, P., Schnakers, C., ... Boly, M. (2010). Default network connectivity reflects the level of consciousness in non-communicative brain-damaged patients. *Brain*, 133(1), 161–171. <http://doi.org/10.1093/brain/awp313>

van Praag, H., Christie, B. R., Sejnowski, T. J., & Gage, F. H. (1999). Running enhances neurogenesis, learning, and long-term potentiation in mice. *Proceedings of the National Academy of Sciences of the United States of America*, 96(23), 13427–13431.

van Praag, H., Kempermann, G., & Gage, F. H. (1999). Running increases cell proliferation and neurogenesis in the adult mouse dentate gyrus. *Nature Neuroscience*, 2(3), 266–270. <http://doi.org/10.1038/6368>

van Praag, H., Shubert, T., Zhao, C., & Gage, F. H. (2005). Exercise enhances learning and hippocampal neurogenesis in aged mice. *The Journal of Neuroscience: The Official Journal of the Society for Neuroscience*, 25(38), 8680–8685.  
<http://doi.org/10.1523/JNEUROSCI.1731-05.2005>

Vidoni, E. D., Honea, R. A., Billinger, S. A., Swerdlow, R. H., & Burns, J. M. (2012). Cardiorespiratory Fitness is Associated with Atrophy in Alzheimer's and Aging Over Two Years. *Neurobiology of Aging*, 33(8), 1624–1632.  
<http://doi.org/10.1016/j.neurobiolaging.2011.03.016>

Voss, M. W., Prakash, R. S., Erickson, K. I., Basak, C., Chaddock, L., Kim, J. S., ... Kramer, A. F. (2010). Plasticity of Brain Networks in a Randomized Intervention Trial of Exercise Training in Older Adults. *Frontiers in Aging Neuroscience*, 2. <http://doi.org/10.3389/fnagi.2010.00032>

Voss, M. W., Weng, T. B., Burzynska, A. Z., Wong, C. N., Cooke, G. E., Clark, R., ... Kramer, A. F. (2015). Fitness, but not physical activity, is related to functional integrity of brain networks associated with aging. *NeuroImage*.  
<http://doi.org/10.1016/j.neuroimage.2015.10.044>

Wang, Y., Risacher, S. L., West, J. D., McDonald, B. C., MaGee, T. R., Farlow, M. R., ... Saykin, A. J. (2013). Altered Default Mode Network Connectivity in Older Adults with Cognitive Complaints and Amnesic Mild Cognitive Impairment. *Journal of Alzheimer's Disease : JAD*, 35(4), 751–760.  
<http://doi.org/10.3233/JAD-130080>

Wei, M., Qin, J., Yan, R., Bi, K., Liu, C., Yao, Z., & Lu, Q. (2015). Association of resting-state network dysfunction with their dynamics of inter-network

interactions in depression. *Journal of Affective Disorders*, 174, 527–534.  
<http://doi.org/10.1016/j.jad.2014.12.020>

Weissman, D. H., Roberts, K. C., Visscher, K. M., & Woldorff, M. G. (2006). The neural bases of momentary lapses in attention. *Nature Neuroscience*, 9(7), 971–978.  
<http://doi.org/10.1038/nn1727>

Whiteman, A. S., Young, D. E., He, X., Chen, T. C., Wagenaar, R. C., Stern, C. E., & Schon, K. (2014). Interaction between serum BDNF and aerobic fitness predicts recognition memory in healthy young adults. *Behavioural Brain Research*, 259, 302–312. <http://doi.org/10.1016/j.bbr.2013.11.023>

Zhou, Z., Ding, M., Chen, Y., Wright, P., Lu, Z., & Liu, Y. (2009). Detecting directional influence in fMRI connectivity analysis using PCA based Granger causality. *Brain Research*, 1289, 22–29. <http://doi.org/10.1016/j.brainres.2009.06.096>

## 6. CURRICULUM VITAE

### **Corey A. Kronman, B.S.**

Year of Birth: 1991

12 Kingsley St, Unit 1

Allston, MA 02134

Telephone: (631) 987-0128

Email: [ckronman@gmail.com](mailto:ckronman@gmail.com)

### **EDUCATION**

---

#### **Boston University School of Medicine, Boston, MA**

Masters of Science, Medical Sciences

Expected May 2016

Concentration: Mental Health Counseling and Behavioral Medicine

GPA 3.53

#### **Boston University College of Engineering, Boston, MA**

Bachelors of Science, Biomedical Engineering

May 2013

GPA 3.20

### **RELEVANT COURSEWORK**

---

Neuroscience • Neuro-engineering • Biomedical Measurements • Molecular Cell Biology & Biotechnology • Signals and Systems • Control Systems • Human Physiology • Bio-transport Phenomenon • Biochemistry • Devices and Diagnostics Design • Thermodynamics & Statistical Mechanics • Group Dynamics & Processing

### **RESEARCH EXPERIENCE**

---

#### **Cardiorespiratory Fitness & Default Mode Network (DMN) Connectivity**

*Mentor: Karin Schon, PhD, Brain Plasticity and Neuroimaging Lab at Boston University*

August 2015-Present

- Assisted in fMRI data collection, fitness testing, and neurocognitive test administration
- Implement functional and effective connectivity analysis on fMRI data
- Applied statistical modeling to correlate fitness and DMN causal influence

#### **Stochastic Resonance (SR) Ankle Brace to Improve Balance Control**

*Mentor: Leia Stirling, PhD, Wyss Institute for Biologically Inspired Engineering*

September 2012-April 2013

- Performed a literature review to determine the primary causes of diminished proprioception
- Designed and constructed the electrical and mechanical systems to safely deliver and control stimulation
- Formulated and implemented a pilot study to determine the effectiveness of the SR ankle brace

## **LEADERSHIP POSITIONS**

---

### **Challenge Course Facilitator, Everwood Day Camp** Summers 2012-2015

- Developed experiential outdoor education programs focusing on communication and team building
- Assisted participants in experiencing personal growth & developing strong interpersonal connections

### **Founder and Current Member, Boston University Parkour** President 2011-2013

- Organized regional competitions and recreational events
- Created a safe community for athletes of varying experience to practice new skills

### **Boston University Cheerleading** Co-Captain 2012-2013; Member 2011-2013

- Collaborated with coaches and team members to sustain a unified, successful team
- Represented Boston University on a national stage

## **KEY SKILLS**

---

Neuroimaging: fMRI Analysis, SPM, GIFT, MarsBaR, REST, xjView, Connectivity Analysis

Computer: Matlab, Python, JMP, LabVIEW, Arduino, Microsoft Office, Linux, Windows, iOS

Research: Data Analysis, Evaluation, & Interpretation, Statistical Computation,

Other: Team Building, Experiential Education, Soldering

## **LANGUAGES**

---

Brazilian Portuguese: Advanced reading and writing comprehension

Spanish: Intermediate reading and writing comprehension